Ore Geology Reviews 158 (2023) 105499

Contents lists available at ScienceDirect

Ore Geology Reviews

journal homepage: www.elsevier.com/locate/oregeorev

Characterising the economic Proterozoic Glyde Package of the greater McArthur Basin, northern Australia

Darwinaji Subarkah [a,b,*], Alan S. Collins [a,b], Juraj Farkaš [b,c], Morgan L. Blades [a], Sarah E. Gilbert [d], Amber J.M. Jarrett [e], Maxwell M. Bullen [a,c], William Giuliano [a,c]

[a] Tectonics & Earth Systems (TES), School of Physics, Chemistry, and Earth Sciences, University of Adelaide, Adelaide, SA 5005, Australia
[b] MinEx CRC, Australian Resources Research Centre, Perth, WA 6151, Australia
[c] Metal Isotope Group (MIG), Department of Earth Sciences, University of Adelaide, Adelaide, SA 5005, Australia
[d] Adelaide Microscopy, University of Adelaide, Adelaide, SA 5005, Australia
[e] Northern Territory Geological Survey, Darwin, NT 0801, Australia

A B S T R A C T

The greater McArthur Basin is an informal term for a Palaeo-to-Mesoproterozoic sedimentary system that consists of terranes from the McArthur Basin, Birrindudu Basin, and the Tomkinson Province. These spatially distant basins are interpreted to connect in the subsurface based on geophysical, lithological, and geochronological evidence. The coeval sedimentary units of the greater McArthur Basin were subdivided into non-genetic depositional 'packages' bookended by regional unconformities. In ascending order, these packages are the: Redbank, Goyder, Glyde, Favenc, and Wilton Packages. The ca. 1660–1610 Ma Glyde Package is the focus of this study and includes the economically important Barney Creek Formation, found in the McArthur Basin *sensu stricto*. The Barney Creek Formation hosts the world-class, sediment-hosted, Zn-Pb-Ag McArthur River deposit. Importantly, it is also a key petroleum source rock and unconventional hydrocarbon reservoir, containing Australia's geologically oldest oil and gas discoveries and forming a part of the McArthur Petroleum Supersystem. Consequently, identifying chronostratigraphically similar units elsewhere in the greater McArthur Basin is important for explorers in finding analogous economic resources.

In situ Rb–Sr geochronological results of the Barney Creek Formation shales sourced from borehole LV09001 yielded ages of 1634 ± 59 Ma and 1635 ± 67 Ma. Shale samples from Fraynes Formation in borehole Manbulloo S1 were dated at 1630 ± 57 Ma and 1636 ± 42 Ma using the same approach. These ages are in good agreement with U–Pb ages of tuffaceous layers from the same units, suggesting that they represent their early burial histories and not secondary, post-depositional events. These results indicate that the Fraynes Formation and the Barney Creek Formation are direct chronostratigraphic equivalents, with ages within analytical error of each other.

In addition to the geochronological similarities, the $\delta^{13}C_{carb,}$ $^{87}Sr/^{86}Sr$, and $\delta^{88/86}Sr$ isotopic constraints from both units also display parallel geochemical fingerprints up-section. These include a positive $\delta^{13}C_{carb}$ excursion of ~2.0 ‰, a trend towards more crustal-dominated $^{87}Sr/^{86}Sr$ ratios, and a negative $\delta^{88/86}Sr$ excursion of ~-0.25 ‰. These findings further support the application of isotopic chemostratigraphy as a powerful tool to correlate distal carbonaceous rocks in the basin system. Importantly, these geochemical fingerprints also show that the McArthur Group and the Limbunya Group experienced similar changes in palaeoenvironments during the evolution of the basin system. However, trace element data collated in this study indicates that they may have recorded different, heterogeneous palaeoredox histories. Geochemical models based on redox-sensitive trace elements V and Mo suggest that the Fraynes Formation sustained a much more euxinic water column as opposed to the Barney Creek Formation. These differences may have implications for the accumulation and preservation of base metals and hydrocarbons within the sediment.

1. Introduction

The informally named McArthur Basin (Fig. 1) is a Palaeoproterozoic to Mesoproterozoic supracontinental sedimentary system unconformably overlying the deformed metamorphosed rocks of the North Australian Craton (Ahmad and Munson, 2013; Close, 2014; Page and Sweet, 1998; Rawlings, 1999). The system extends over 180,000 km^2 across northern Australia (Ahmad and Munson, 2013; Page and Sweet, 1998; Rawlings, 1999), from the borders of Western Australia into northwestern Queensland (Fig. 1). The greater McArthur Basin consists of sedimentary rocks of the McArthur Basin *sensu stricto*, the Birrindudu Basin, and the Tomkinson Province (Close, 2014). These far-separated successions have been interpreted to be continuous in the subsurface based on seismic (Blaikie and Kunzmann, 2017, 2019; Blaikie and Kunzmann, 2020; Debacker et al., 2021; Frogtech Geoscience, 2018; Hoffman, 2014; Munday et al.; Plumb and Wellman, 1987; Sheldon et al., 2021), sedimentological (Jarrett et al., 2022; Kunzmann et al., 2022; Kunzmann et al., 2020; Kunzmann et al., 2019; Page et al., 2000;

* Corresponding author.
E-mail address: Darwinaji.subarkah@adelaide.edu.au (D. Subarkah).

https://doi.org/10.1016/j.oregeorev.2023.105499
Received 25 October 2022; Received in revised form 12 May 2023; Accepted 22 May 2023
Available online 24 May 2023
0169-1368/© 2023 The Author(s). Published by Elsevier B.V. This is an open access article under the CC BY license (http://creativecommons.org/licenses/by/4.0/).

Rawlings, 2002; Rawlings, 1999; Schmid, 2015; Smith, 2016), and geochronological findings (Bodorkos et al., 2022; Munson, 2019; Nixon et al., 2021; Page et al., 2000; Page and Sweet, 1998; Yang et al., 2022). The sedimentary units of the greater McArthur Basin were categorised into five, basin-scale, non-depositional packages based on their lithostratigraphy, age, composition of volcanism, and basin-fill geometry (Ahmad and Munson, 2013; Close, 2014; Rawlings, 1999). In stratigraphic order, these are the Redbank, Goyder, Glyde, Favenc, and Wilton Packages.

The Glyde Package is the focus of this study and hosts the world-class McArthur River Zn-Pb-Ag deposit that forms part of the Carpentaria Zn belt in northern Australia (Huston et al., 2006; Large et al., 2005; Leach et al., 2005; Porter, 2017). This package have been interpreted to be chronostratigraphically equivalent to the Loretta and River Supersequences within the Isa Superbasin and the McNamara Group in the Lawn Hill Platform (Krassay et al., 2000; McGoldrick et al., 2010; Page et al., 2000; Page and Sweet, 1998; Southgate et al., 2000). Mineralisation in the McArthur River is also known as the 'Here's Your Chance (HYC)' deposit, and is commonly stratabound along pyritic, carbonaceous, shale units. (Croxford et al., 1975; Kunzmann et al., 2019; Large et al., 1998; Large et al., 2000; Large et al., 2005). Pre-mining evaluation estimated that the HYC deposit contains 237 million tonnes of potential resources at 9.2% Zn, 4.1% Pb, and 41 ppm Ag (Gustafson and Williams, 1981; Porter, 2017). The HYC deposit is impressively well preserved, showing little evidence of deformation or metamorphism (Large et al., 2005; Spinks et al., 2021).

In addition, the Barney Creek Formation and their equivalent units also constitutes the prospective McArthur Petroleum Supersystem (Bradshaw, 1994; Jarrett et al., 2022). The McArthur Petroleum Supersystem contains Australia's geologically oldest conventional and unconventional oil and gas discoveries (Croon et al., 2015; Jackson et al., 1986). The region continues to be promising, with wells intersecting the province exhibiting both oil bleeds and gas shows (Crick et al., 1988; Croon et al., 2015; Jackson et al., 1988; Jackson et al., 1986; Jarrett et al., 2022; Kovac et al., 2014). Fourteen potential source rocks have been identified within the McArthur Petroleum Supersystem, many with very good to excellent organic richness (Jarrett et al., 2022). Many of the shales within this division are thermally mature, in the zone of oil and gas formation (Jarvie and Breyer, 2011). As such, establishing a chronological framework of equivalent units to the Barney Creek Formation would assist for explorers in finding similar plays. Furthermore, constraining how the palaeoenvironment and water chemistry of the

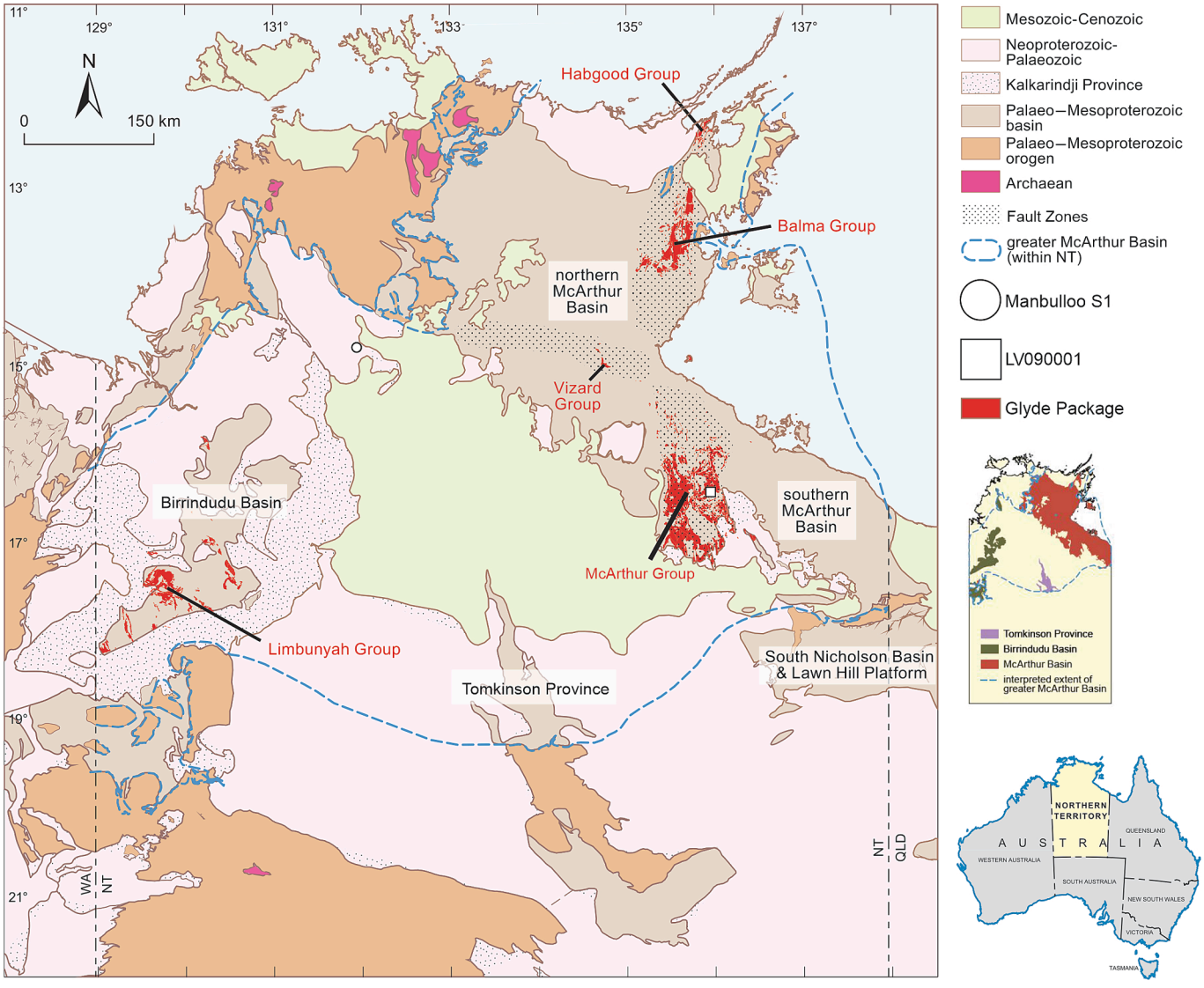

Fig. 1. Geological map of the greater McArthur Basin as defined by Close (2014) with the outcropping components of the Glyde Package (Munson, 2019) and the localities of boreholes used in this study. The Northern Territory geological regions are sourced from the Northern Territory Geological Survey's 1:2.5 M Geographic Information System dataset and can be found in https://geoscience.nt.gov.au/gemis/ntgsjspui/ and http://strike.nt.gov.au/wss.html.

Barney Creek Formation and its coeval units would also assist in understanding the formation, accumulation, and preservation of other potential base-metal mineralisation and hydrocarbon reservoirs.

Notably, previous investigators have also shown that the greater McArthur Basin was potentially part of a large, inter-continental seaway (Collins et al., 2019; Cox et al., 2022; Gibson et al., 2018; Kirscher et al., 2020; Pisarevsky et al., 2014; Wang et al., 2019; Zhang et al., 2012). Palaeomagnetic findings have suggested that northern Australia bordered other continents such as North China (Wang et al., 2019; Zhang et al., 2012), Baltica (Hamilton and Buchan, 2010; Karlstrom et al., 2001; Zhao et al., 2004), and Laurentia (Karlstrom et al., 2001; Kirscher et al., 2020; Medig et al., 2014) during the Proterozoic. This palaeogeographical link is further corroborated by the similarities in lithostratigraphy (Kunzmann et al., 2019; Yang et al., 2019; Zhang et al., 2021), basin provenance (Ding et al., 2017; Lu et al., 2008; Nordsvan et al., 2018; Yang et al., 2018; Zhang et al., 2022), igneous activity (Bodorkos et al., 2022; Nixon et al., 2021; Zhang et al., 2018; Zhang et al., 2017), astrochronological constraints (Mitchell et al., 2020), sediment-hosted mineralisation (Gianfriddo et al., 2022; Gibson et al., 2017; Gu et al., 2012; Southgate et al., 2000; Wang et al., 2014), and petroleum plays (Cox et al., 2022; Craig et al., 2013; Jarrett et al., 2022; Liu et al., 2011; Wenzhi et al., 2018; Yang et al., 2020). As such, this sedimentary system may be critical for global scale palaeoenvironment reconstructions during the Palaeoproterozoic (Cox et al., 2016; Cox et al., 2019; Jarrett et al., 2019; Johnston et al., 2008; Lyons et al., 2014; Mukherjee and Large, 2020; Shen et al., 2002; Vinnichenko et al., 2020). In particular, the Glyde Package has historically been studied as a key section for understanding early biological life, palaeowater, and atmospheric chemistry ca. 1.6 Ga (Brocks et al., 2005; French et al., 2020; Kunzmann et al., 2019; Mukherjee et al., 2019; Oehler, 1977; Stüeken et al., 2021). Consequently, the findings from this study can also be used to help expand upon how surface environments evolved during this period.

In order to help characterise the extent of the economic Glyde Package, we look to establish a chronological framework and chemostratigraphic correlations between distal successions in the sedimentary system. In particular, this study focuses on the McArthur Group sourced from well LV09001 in the McArthur Basin *sensu stricto,* and the Limbunya Group from well Manbulloo S1 in the Birrindudu Basin. Shale-hosted clay minerals from both groups were dated using *in situ* Rb–Sr geochronology to bracket the depositional window of the units. Furthermore, chemical signatures of marine sedimentary rocks here were investigated using a multi-proxy approach to understand how the palaeoenvironment and palaeoredox history of the Glyde Package evolved. Correlating any geochemical excursions would suggest that the complex tectonic /hydrographic regime of the sedimentary system is extensively recorded in both the McArthur Basin and the Birrindudu Basin. As a result, this would suggest that the under-explored Birrindudu Basin can also potentially host analogous economic potential that is present in the McArthur Basin.

2. Background

The McArthur Group units from the southern McArthur Basin along with the Vizard and Habgood Groups from the northern McArthur Basin forms the McArthur Basin *sensu stricto* successions (Fig. 1) of the Glyde Package (Ahmad and Munson, 2013; Close, 2014; Rawlings, 1999). A maximum depositional constraint for the lower McArthur Group is defined by a green tuffaceous siltstone from the Mallapunyah Formation which gave an age of 1653 ± 17 Ma (Ahmad and Munson, 2013; Page et al., 2000). Direct sensitive high-resolution ion microprobe (SHRIMP) U–Pb dating of volcanic zircons from tuffites in the Barney Creek Formation have yielded ages of 1640 ± 4, 1639 ± 3, and 1638 ± 7 Ma (Page et al., 2000; Page and Sweet, 1998). These results are interpreted to be the absolute depositional age of the unit (Munson, 2019). Lastly, another tuff layer from the unconformably overlying Balbirini Dolosotone gave a SHRIMP U–Pb age of 1589 ± 3 Ma (Page et al., 2000), bookending the depositional window for the McArthur Group. These ages are well correlated with those from the Limbunya Group, which forms the Birrindudu Basin successions of the Glyde Package (Close, 2014; Cutovinos et al., 2002; Munson, 2019; Munson et al., 2020; Smith, 2001). A detrital zircon analysis from the Farquharson Sandstone resulted in a maximum depositional age of 1654 ± 12 Ma for the lower Limbunya Group (Kositcin and Carson, 2017). In addition, recent dating of tuff layers from the Fraynes Formation gave an age of 1642 ± 4 Ma, suggesting that this unit is directly correlative to the Barney Creek Formation (Munson et al., 2020). These correlations and age constraints are summarised in Fig. 2.

2.1. Geological setting of the McArthur Group, McArthur Basin

The McArthur Group is categorised into two sub-groups (Jackson et al., 1987; Plumb and Wellman, 1987): the older Umbolooga Subgroup and the overlying Batten Subgroup (Fig. 2). The Emmerugga Dolostone from the Umbolooga Subgroup is the oldest unit of the McArthur Group in this study. The formation is divided into two members: the Mara Dolostone Member and the Mitchell Yard Dolostone Member (Pietsch, 1991; Winefield, 1999). The Mara Dolostone Member is primarily a stromatolitic dolarenite, with common occurrences of columnar, domal, and conical stromatolites (Ahmad and Munson, 2013). The Mitchell Yard Dolostone Member conformably overlies the Mara Dolostone Member and is instead more massive and featureless (Ahmad and Munson, 2013). These sections thicken up-section and were interpreted to have been deposited in a tidal to deep marine environment on an intracratonic carbonate platform (Ahmad and Munson, 2013; Winefield, 1999). The Teena Dolostone is younger than the Emmeruga Dolostone, and tuff layers within the unit have been dated at 1639 ± 6 Ma (Page et al., 2000). The unit recorded a shallowing cycle up stratigraphy, with the youngest sections containing oolitic grainstone, rippled and laminated dolarenite, and thin beds of carbonaceous shale (Ahmad and Munson, 2013). Notably, the radiating fans of vertical dolomite crystals called the 'Coxco Needles' regularly occur in the Teena Dolostone (Jackson et al., 1987; Walker et al., 1977; Winefield, 2000). Similar pseudomorphs in coeval units from the greater McArthur Basin and other Palaeoproterozoic basins in northern Australia have also been observed, and they are used as a key feature to correlate units that are spatially apart (Ahmad and Munson, 2013). The Barney Creek Formation unconformably overlies the Teena Dolostone and is largely a recessive unit (Ahmad and Munson, 2013; Jackson et al., 1987; Kunzmann et al., 2022; Rawlings, 1999). The succession comprises of finely laminated to thinly bedded carbonaceous and pyritic siltstone, dololutite, and locally abundant tuff beds. The HYC Pyritic Shale Member here is continuously recessive and hosts the world-class Zn-Pb-Ag deposit (Eldridge et al., 1993; Large et al., 1998; Pietsch, 1991). The Barney Creek Formation has been interpreted to represent deep-water shaley carbonates deposited during the maximum flooding of a sea-level transgression (Bull, 1998; Kunzmann et al., 2019; Winefield, 1999). However, it should be noted that the Barney Creek Formation records significant differences in lateral facies and thicknesses across the McArthur Basin (Kunzmann et al., 2022). These differences are likely induced by a geographic shift in the depocentre that occurred during the structural re-organisation of the basin (Kunzmann et al., 2022). The overlying Reward Dolostone represents an upward-shallowing cycle after the deposition of the Barney Creek Formation (Ahmad and Munson, 2013; Kunzmann et al., 2022; Kunzmann et al., 2019). The depositional environment for the unit is likely to be locally high-energy to peritidal, with sections of stromatolitic dololutite to massive, cross-bedded sandstone (Haines, 1994; Pietsch, 1991). The lower contact with the Barney Creek Formation is commonly conformable and gradational, but locally disconformable where palaeo-regolith develops (Pietsch, 1991).

The Batten Subgroup (Fig. 2) unconformably overlies the Reward

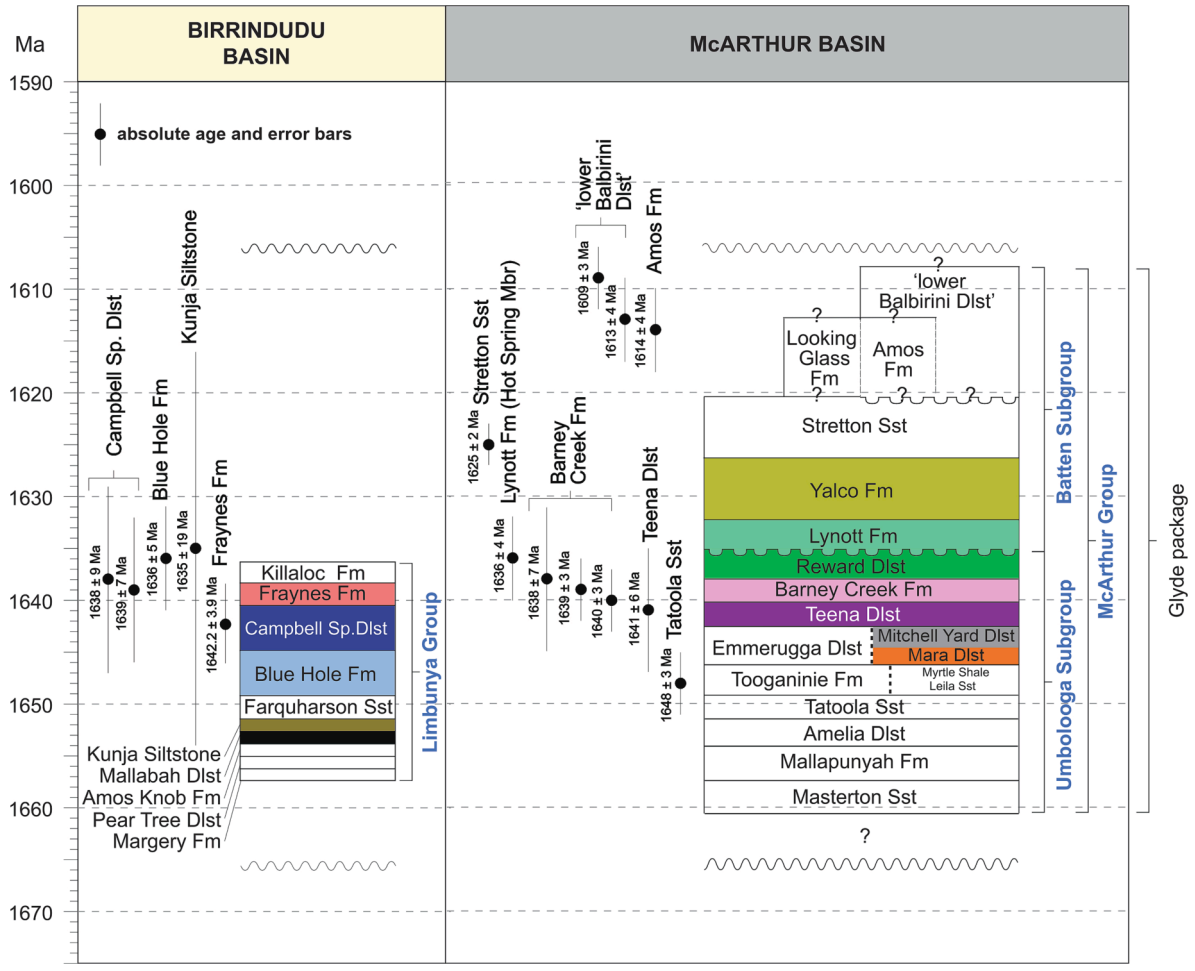

Fig. 2. Stratigraphic correlation of the Glyde Package units from the McArthur Basin and the Birrindudu Basin adapted from Munson (2019) based on U–Pb dating of tuff layers in the corresponding formations (Kositcin and Carson, 2017; Munson et al., 2020; Page et al., 2000; Page and Sweet, 1998).

Dolostone (Jackson et al., 1987; Plumb and Wellman, 1987) and largely consists of shallower sequences than the Umbolooga Subgroup (Ahmad and Munson, 2013). The Lynott Formation is evaporitic, consisting of dolomitic siltstone, stromatolitic dolostone, and sandstone (Jackson et al., 1987). The uppermost section of the unit comprises of abundant cauliflower chert, suggesting that it was deposited in a supratidal to sabkha setting (Pietsch, 1991). A tuff-layer from the top of the Lynott Formation returned an age of 1636 ± 4 Ma overlapping with the Barney Creek Formation (Page et al., 2000), suggesting that the unconformity with the Batten Subgroup represents a short period of time. The following Yalco Formation is the youngest unit from the McArthur Group investigated in this study. The succession is commonly interbedded with stromatolitic dolarenite and rippled sandstone (Ahmad and Munson, 2013). Sedimentary structures such as ripple marks, desiccation cracks, and casts of evaporitic minerals further suggests that the unit was deposited in a shallow-marine environment that experienced intermittent emergence (Jackson et al., 1987; Pietsch, 1991). The McArthur Group samples here were sourced from the LV09001 drill hole (Fig. 1).

2.2. Geological setting of the Limbunya Group, Birrindudu Basin

The Mallabah Dolostone is the oldest unit from the Limbunya Group (Fig. 2) that is assessed in this study. It comprises of laminated, stromatolitic dolostone fining upwards into dolomitic mudstone (Ahmad and Munson, 2013; Cutovinos et al., 2002). Sequences from the Mallabah Dolostone suggest a transition from shallow-marine conditions towards more lower-energy, deeper marine environments potentially below the wave base (Cutovinos et al., 2002). This marine environment is further reflected by the sedimentology of the overlying Kunja Siltstone which is dominated by laminated mudstone and fissile silts (Cutovinos et al., 2002). Consequently, the Kunja Siltstone has been interpreted to represent a maximum flooding surface (Ahmad and Munson, 2013). Tuff layers from this formation have yielded a U–Pb zircon age of 1635 ± 19 Ma (Fanning, 1991). Previous investigators have also noted elevated organic carbon content and concentrations of Pb and Zn within the formation (Cutovinos et al., 2002), with a maximum TOC of 2.1 wt% (Jarrett et al., 2022). The conformably overlying Farquharson Sandstone mainly consists of blocky, massive sandstone and depicts a change back into shallower environments (Ahmad and Munson, 2013) but is not sampled here.

The following Blue Hole Formation and Campbell Springs Dolostone are lithologically similar, comprising of dolomitic mudstone and siltstone as well as stromatolitic dolostone (Cutovinos et al., 2002; Dunster, 1998). However, they are separated by a distinctive purple interbed with hemispherical, bioherms of digitate stromatolites (Ahmad and Munson, 2013). Importantly, acicular crystal pseudomorphs identical to the Coxco Needles found in the Teena Dolostone are commonly abundant in the Blue Hole Formation and the Campbell Springs Dolostone (Sweet et al., 1974). Furthermore, a tuff U–Pb zircon age from the Campbell Springs Dolostone yielded 1638 ± 9 Ma (Cutovinos et al., 2002). This is in good agreement with an age from the Teena Dolostone in the McArthur Basin (Page et al., 2000), suggesting that they are directly correlative units. These correlations are further supported by the overlying

Fraynes Formation, which consists of micaceous siltstone with more carbonate interbeds up-section (Sweet et al., 1974). The Fraynes Formation is correlated with the Barney Creek Formation of the McArthur basin and is interpreted to have been deposited in a nearshore shallow-marine environment with intermittent periods of deeper-marine phases (Cutovinos et al., 2002). The Limbunya Group samples here were sourced from the Manbulloo S1 drill hole (Fig. 1).

3. Methodologies

The methods and subsequent reference materials used in this study are summarised here and discussed further in the Supplementary Material. Geochemical data from literature were also compiled in this study and their methodologies can be found in the references therein (Bruisten and Brocks, 2015; Jarrett et al., 2018; Jarrett et al., 2021; NTGS., 2015; Vinnichenko and Brocks, 2019; Vinnichenko et al., 2021).

3.1. Shale geochemical analysis

Shale samples were washed to rid of surface contaminants and were finely powdered using a tungsten carbide mill at the University of Adelaide. Organic geochemical data were collected by pyrolysis analysis of raw powdered samples by a Weatherford's Source Rock Analyser following Cox et al. (2016). The flame ionisation detector (FID) was calibrated with a Weatherford Laboratories Instruments Division Standard 533 and analysers were regulated against a standard gas with known concentration of CO_2 and CO. Results were processed with Optkin 3.0 software, where peaks and geochemical indices such as total organic carbon (TOC), Oxygen Index (OI), Hydrogen Index, and Production Index (PI) are automatically calculated. They were then screened using the criteria defined by Hall et al. (2016). Major, trace, and rare earth and yttrium element (REEY) analyses were collected at Bureau Veritas using an Agilent 7900 Series Inductively Coupled Plasma-Mass Spectrometer (ICP-MS).

3.2. Carbonate geochemical analysis

Major, trace, and REEY concentrations from carbonate rocks here were determined following Kuznetsov et al. (2010) to minimise non-authigenic, secondary phases from the bulk sediment. Homogeneous carbonate laminations were micro-drilled and their following rock powder washed with ammonium acetate to remove loosely bounded cations. Further leaching was then done using dilute ammonium acetate and acetic acid to extract the primary carbonate phase. Elemental concentrations were then analysed on the final solutions using an Agilent 8900 ICP-MS/MS operated in solution mode at Adelaide Microscopy.

Radiogenic and stable Sr isotopic analyses were undertaken on an aliquot of the sample solution prepared for elemental geochemistry of bulk carbonates. The coupled $^{87}Sr/^{86}Sr$ and $\delta^{88/86}Sr$ determinations were completed at the University of Adelaide using a Phoenix Isotopx thermal ionisation mass spectrometry (TIMS) instrument following Shao et al. (2021). Briefly, two aliquots (i.e., spiked and unspiked) were taken from a sample solution to define the $\delta^{88/86}Sr$ values in samples. One of the aliquots was spiked using an ^{87}Sr-^{84}Sr double spike solution, with the resulting Sr fraction separated via ion chromatography using Sr-Spec micro-columns. Pure Sr fractions were then loaded on single non-zone-refined rhenium filaments for TIMS analysis. The unspiked aliquots were purified using the same approach and ran on the same instrument using a multi-dynamic peak-hopping method (Shao et al., 2021) for radiogenic $^{87}Sr/^{86}Sr$ ratios. The standard reference materials SRM 987 and JCP-1 were used for this procedure (Balcaen et al., 2005; Krabbenhöft et al., 2009; Shao et al., 2021). The $\delta^{13}C$ and $\delta^{18}O$ isotopic signature in carbonates were collected following Spötl and Vennemann (2003). In short, micro-drilled rock powder samples were placed into glass vials, purged with phosphoric acid, and injected with helium. The ratio of the isotopic composition from the resultant gas was measured using a Dual Inlet Isotope Ratio Mass Spectrometer (DI-IRMS) with attached Fissions Isocarb Carbonate Preparation System at the University of Adelaide. These values are expressed as relative to Pee Dee Belemnite values using internal working standards.

3.3. High resolution imaging and in situ Rb–Sr dating with trace element analysis of shales

Shale samples prepared for *in situ* Rb–Sr dating and trace element analysis were first mapped for their petrographic textures and elemental composition. This was done using an FEI Quanta 450 Scanning Electron Microscope (SEM) with attached Oxford Ultima Max Large Area SDD EDS detector at Adelaide Microscopy following Subarkah et al. (2021). The images were processed using the Oxford Aztec EDS software. Detrital, replacement, and non-K-bearing minerals were avoided for *in situ* Rb–Sr analysis to avoid incorporating non-authigenic phases.

In situ Rb–Sr analyses were performed at Adelaide Microscopy following the approach described by Redaa et al. (2021a) using an Agilent 8900 ICP-MS/MS instrument coupled to a RESOlution ArF 193 nm excimer laser ablation system. Each spot analysis consisted of 20 s of gas background collected while the laser was not firing, followed by 40 s of ablation time. A reaction gas N_2O was introduced in the reaction chamber. This compound oxidises the Sr ion forming $^{87}Sr^{16}O$. This allows the reaction product to be measured without mass interference with ^{87}Rb. Laser and mass spectrometer parameters used here are summarised in the Supplementary Information. All samples were analysed using a 67 μm laser beam, 5 Hz repetition rate and a fluence of 3.5 J/cm^2. Targeting a mixture of several clay-sized, cogenetic minerals in one ablation spot using the same approach have proven to yield robust isochrons and ages (Subarkah et al., 2021; Subarkah et al., 2022; Tillberg et al., 2020). Phlogopite nano-powder Mica-Mg was used as the primary reference material for Rb/Sr (Govindaraju et al., 1994) and the synthetic reference glass NIST610 (Hogmalm et al., 2017; Woodhead and Hergt, 2001) for normalisation of Sr/Sr ratios and trace elements. The natural phologpite mineral crystal MDC sourced from the same location as Mica-Mg (Govindaraju et al., 1994) and glauconite sample GL-O of known Cretaceous age from Bagnols-sur-Cèze, France were also analysed as secondary age standards during the same run (Rousset et al., 2004). In addition, basalt standard BCR-2G was also used as a secondary standard to cross-check elemental quantification (Jochum et al., 2005; Wilson, 1997). Laser ablation data and error correlations were processed using the LADR software package (Norris and Danyushevsky, 2018; Schmitz and Schoene, 2007). During the data-processing, Zr, Si, Ti, and REEY signals were monitored to filter the non-authigenic component in each ablation analysis (Subarkah et al., 2022). Non-stable isotopic and elemental signatures were also screened during the process to ensure spot homogeneity. Isochron ages and initial $^{87}Sr/^{86}Sr$ ratios were calculated using IsoplotR (Vermeesch, 2018). Geochronological errors reported in this study are 2σ.

4. Results

Three runs of JCP-1 yielded a mean value of 0.190 ± 0.012 for stable $\delta^{88/86}Sr$ ratios and 0.709157 ± 0.000005 for $^{87}Sr/^{86}Sr$ isotopes respectively. These results are accurate to the published values ($\delta^{88/86}Sr$: 0.197 ± 0.013, $^{87}Sr/^{86}Sr$: 0.709164 ± 0.000006) of the standard (Krabbenhöft et al., 2009). Next, the SRM 987 gave a mean $\delta^{88/86}Sr$ value of 0.028 ± 0.050 and $^{87}Sr/^{86}Sr$ value of 0.710253 ± 0.000003. This is also in good agreement with their respective data ($\delta^{88/86}Sr$: 0.012 ± 0.044, $^{87}Sr/^{86}Sr$: 0.710250 ± 0.000010) found in literature (Balcaen et al., 2005; Krabbenhöft et al., 2009). Mean values of major, trace and REEY in BCR-2G here are also within error and positively correlates (Pearson $R^2 > 0.999$, Pearson $R^2 > 0.999$, and P Value < 0.0001) with their published record (Jochum et al., 2016; Jochum et al., 2005; Wilson, 1997).

Reference material Mica-Mg (Govindaraju et al., 1994) prepared

here as a nano-powder pellet and a phlogopite sample MDC sourced from the same location were used a primary and secondary standards for *in situ* Rb–Sr geochronology respectively (Hogmalm et al., 2017; Jegal et al., 2022; Redaa et al., 2021a). These standards have been used jointly and are assumed to be of the same age (Armistead et al., 2020; Hogmalm et al., 2017; Li et al., 2020; Redaa et al., 2021a; Redaa et al., 2021b; Subarkah et al., 2022; Tamblyn et al., 2020). The standards Mica-Mg and MDC were anchored to its reported $^{87}Sr/^{86}Sr$ value of 0.72607 ± 0.00363 (Hogmalm et al., 2017) and gave an age of 522 ± 4 and 529 ± 6 Ma, respectively. This is within error of the average age of the source rocks at 519 ± 7 Ma (Hogmalm et al., 2017). The glauconite GL-O secondary standard (Rousset et al., 2004) analysed here gave an age of 94 ± 3 Ma, accurate to its published K–Ar age of 95 ± 1.5 Ma (Derkowski et al., 2009). It should be noted that the age of GL-O is consistently younger than the age of the rock (113 ± 0.3 Ma) it is hosted in (Selby, 2009). Consequently, the ages yielded from GL-O have been interpreted to instead time the glauconite formation after the deposition of its host rock (Selby, 2009). Further discussions of the results used in this study can be found in the Supplementary Material.

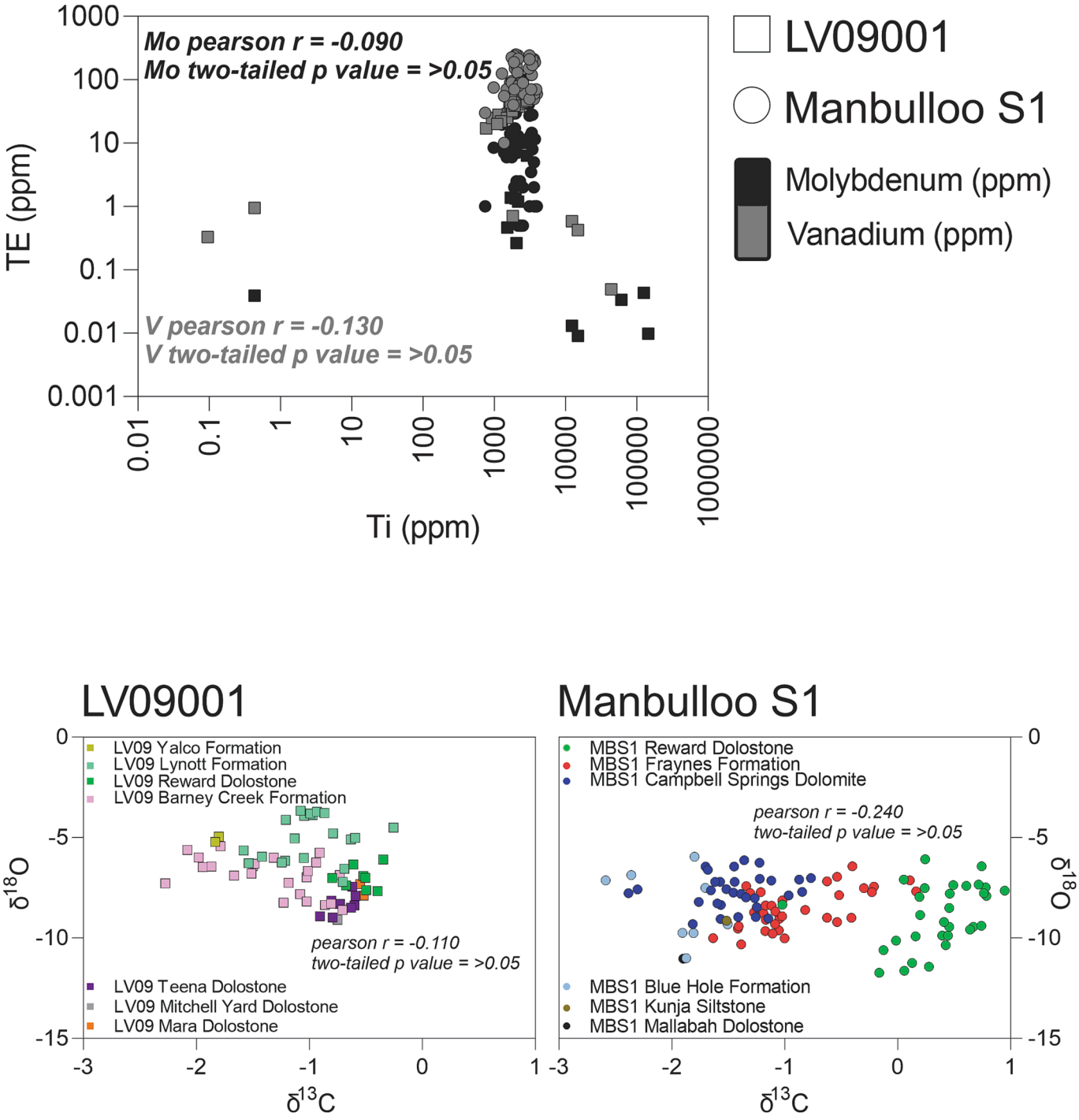

Fig. 3. Geochemical proxies for detrital contamination (Reinhard et al., 2013) and alteration (Banner and Hanson, 1990) plotted against the palaeoenvironmental indicators used in this study show no statistically significant relationship between the variables.

4.1. Whole-rock shale and carbonate geochemistry of the Glyde Package

The chemical signatures of marine sedimentary rocks have been applied to help elucidate past earth systems processes interacting on our planet's surface. However, it is crucial to show that the chemical fingerprints used for further interpretations represent the authigenic component of these rocks. For example, the geochemical composition of whole-rock samples in this study may be influenced by detrital input, and its trace element budget may be dominated by this detrital component. As such, Titanium (Ti) is used here (Fig. 3) and elsewhere (Reinhard et al., 2013) as an index element to fingerprint increasing detrital flux into marine sedimentary rocks. Consequently, relationships between Ti and trace elements may suggest a significant influence on the geochemical signature of these samples (Goodarzi et al., 2019; Reinhard et al., 2013; Schier et al., 2021; Tostevin et al., 2016). Here, Ti content and trace element composition display no statistically significant co-variations (Fig. 3). As such, detrital contamination is considered to be minimal in the results observed in this study.

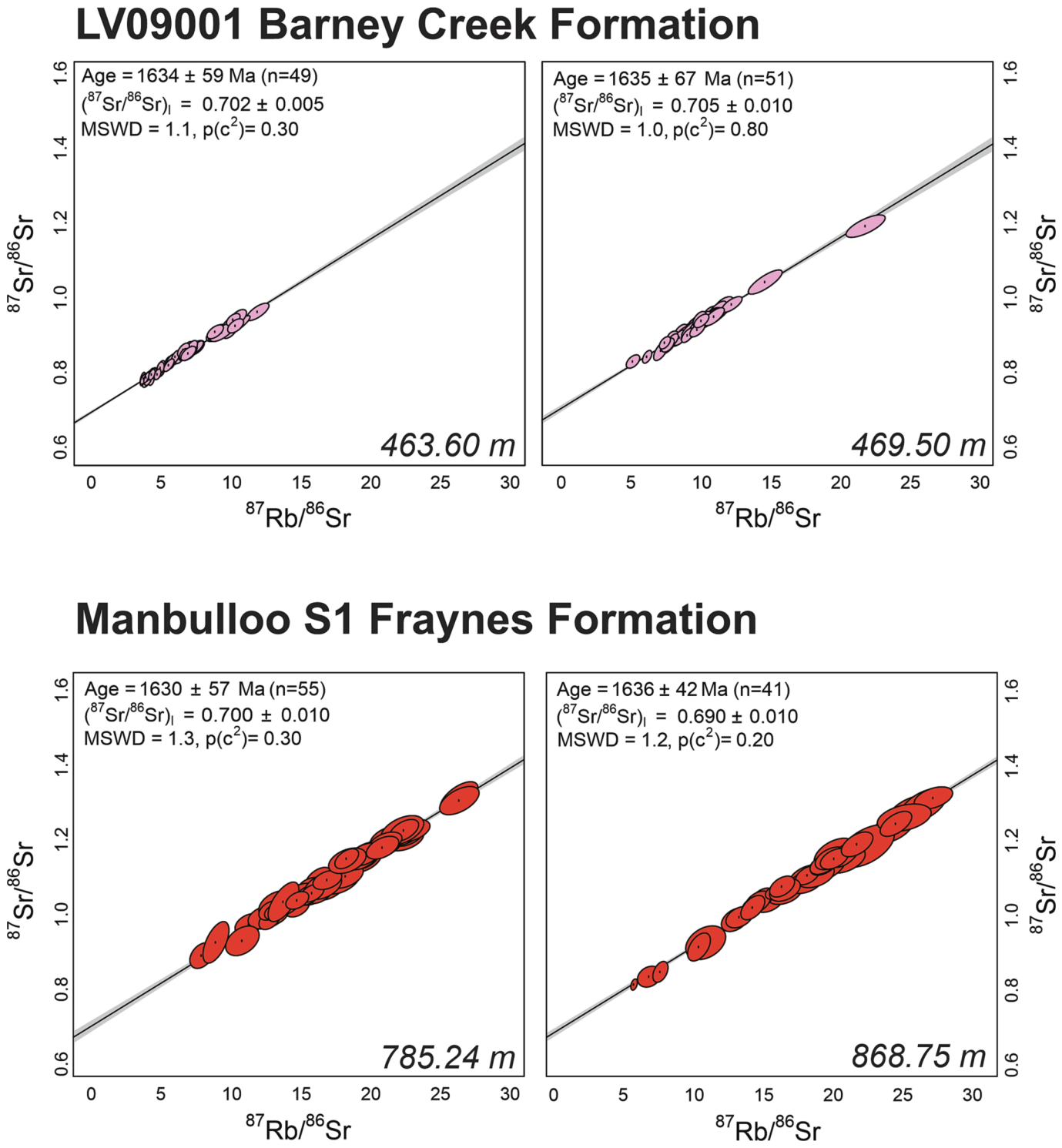

Fig. 4. *In situ* Rb–Sr geochronological results from shales in the Barney Creek Formation and Fraynes Formation sourced from boreholes LV09001 and Manbulloo S1, respectively.

Furthermore, geochemical signatures may be affected by post-depositional diagenetic alteration (Allan and Matthews, 1982; Banner and Hanson, 1990; Degens and Epstein, 1962; Killingley, 1983; Land, 1995). Such secondary reactions are commonly screened by identifying relationships (Fig. 3) between the $\delta^{13}C$ and $\delta^{18}O$ isotopic systems (Allan and Matthews, 1982; Banner and Hanson, 1990). Samples from both wells show no significant correlations between these two isotopes (Fig. 3). In addition, anomalously light $\delta^{18}O$ values have been suggested to be caused by geochemical overprinting from meteoric waters or elevated temperatures (Degens and Epstein, 1962; Killingley, 1983; Land, 1995). All of the $\delta^{18}O$ isotopic results here are heavier than −15‰ (Fig. 3). Together, the lack of detrital input and the absence of diagenetic overprinting suggest that the geochemistry of these samples reflect the coeval basin water composition during their formation in the Proterozoic. The isotopic signatures from the Fraynes Formation and the Barney Creek Formation display the best correlations with each other (Fig. 7). This includes a positive $\delta^{13}C_{carb}$ excursion of 2.0‰, fluctuations in $^{87}Sr/^{86}Sr$ up-section, and a negative $\delta^{88/86}Sr$ excursion of −0.25‰. However, it should be a notably less amount of Sr isotope data when compared to the C isotope data. As such, there is a higher confidence in the interpreted correlations for the Glyde Pacakge based on their $\delta^{13}C$ chemostratigraphy as opposed to the other isotopic systems here.

The Fraynes Formation here yielded the most variable TOC and redox-sensitive proxies (Figs. 5 and 6). This heterogeneity is similarly mirrored by findings from the Barney Creek Formation. On the other hand, the trace element indicators from Campbell Springs Dolostone and the Teena Dolostone are more homogeneous (Fig. 6). Notably, samples from the Reward Dolostone, and the Lynott Formation consistently had lower average redox index element concentrations in comparison to the other units studied here (Fig. 6). The whole-rock geochemical data collected is summarised in Table 1.

4.2. High-resolution petrographic mapping of shales from the Barney Creek Formation and the Fraynes Formation

Prior to laser analysis, samples were mapped for their petrographic relationships (Supplementary Material and Supplementary Figure 4). The finest-grained, homogeneous, black laminations of each sample were targeted to avoid detrital contamination, obvious alteration assemblages, and veining. Clay minerals from the Barney Creek Formation in well LV09001 and the Fraynes Formation from Manbulloo S1 had similar morphologies. These minerals do not exhibit characteristics commonly found in detrital clays such as angular, fragmented boundaries, large grain sizes, and textural immaturity (Deepak et al., 2022; Rafiei and Kennedy, 2019; Rafiei et al., 2020). Instead, they look to form in the sediment as an authigenic assemblage along with quartz. A Barney Creek Formation shale sample from depth 463.60 m shows fine illite flakes concentrated in mottled domains, with sections where individual flakes cannot be distinguished (Supplementary Material). Concentrations of illite commonly preserve their compaction structures, wrapping around detrital quartz grains. A sample of the same unit from depth 469.50 m still displays primary bedding structures. Illite minerals here are interconnected, filling pore spaces and grow together with quartz cement. These clay morphologies are similarly displayed in the Fraynes Formation shale samples from Manbulloo S1. Furthermore, early diagenetic pyrite can be observed growing together with siderite. Altogether, these petrographic relationships suggest the authigenic formation of clay minerals within the sediment (Deepak et al., 2022; Kennedy et al., 2006; Kennedy et al., 2002; Rafiei and Kennedy, 2019; Rafiei et al., 2020; Subarkah et al., 2021). Consequently, the Rb–Sr data collected in this study should derive from these authigenic or early diagenetic K-rich (and as such Rb-bearing) illite phases, providing the minimum age constraint of these formations.

4.3. Rb–Sr geochronology of distal shale samples from the Glyde Package

In situ Rb–Sr geochronology of shale samples from the Glyde Package

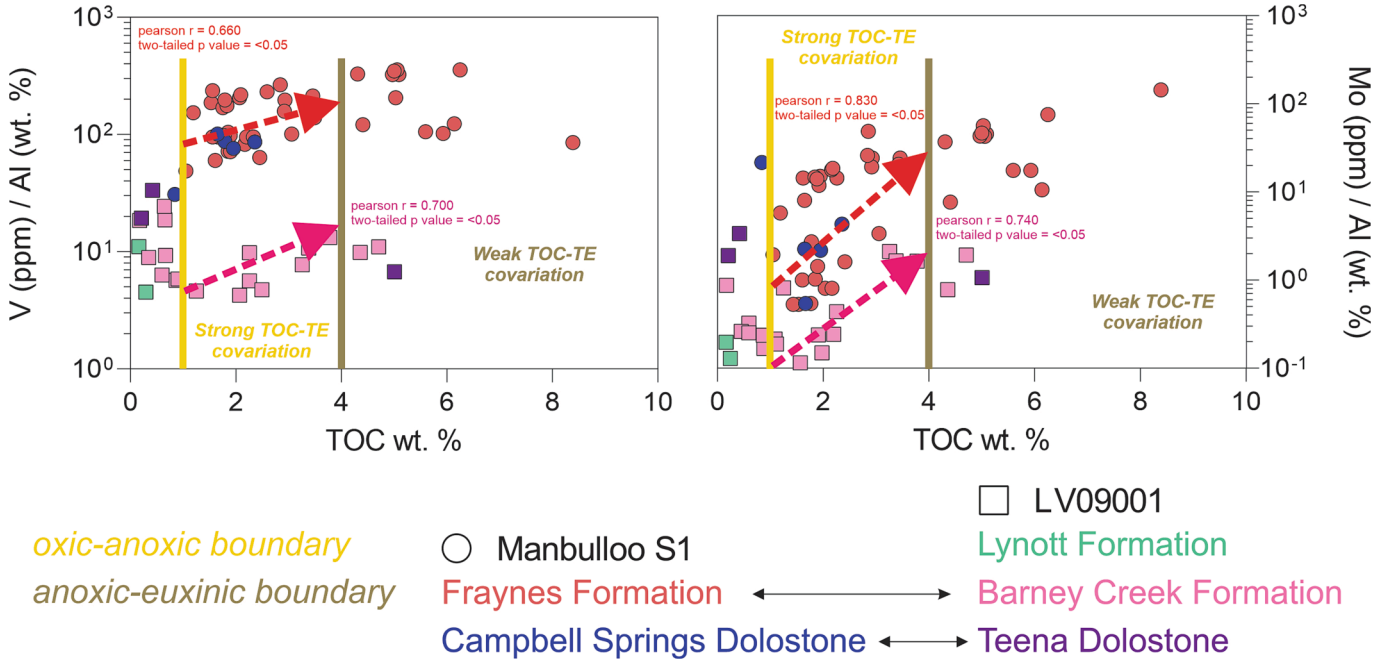

Fig. 5. Redox-sensitive trace element enrichments with respect to total organic carbon (TOC) content. Note that V and Mo both show similar patterns, with strong linear relationships with TOC between 1 and 4 wt%. These thresholds are similarly found elsewhere in sections of the greater McArthur Basin with excellent hydrocarbon reservoir potential (Cox et al., 2016). This positive covariation and its subsequent breakdown at TOC content above 4 wt% is consistent with the onset of anoxia followed by intermittent euxinia (Algeo and Maynard, 2004; Scott and Lyons, 2012). Note that the Fraynes Formation show a stronger affinity for euxinic conditions compared to the Barney Creek Formation.

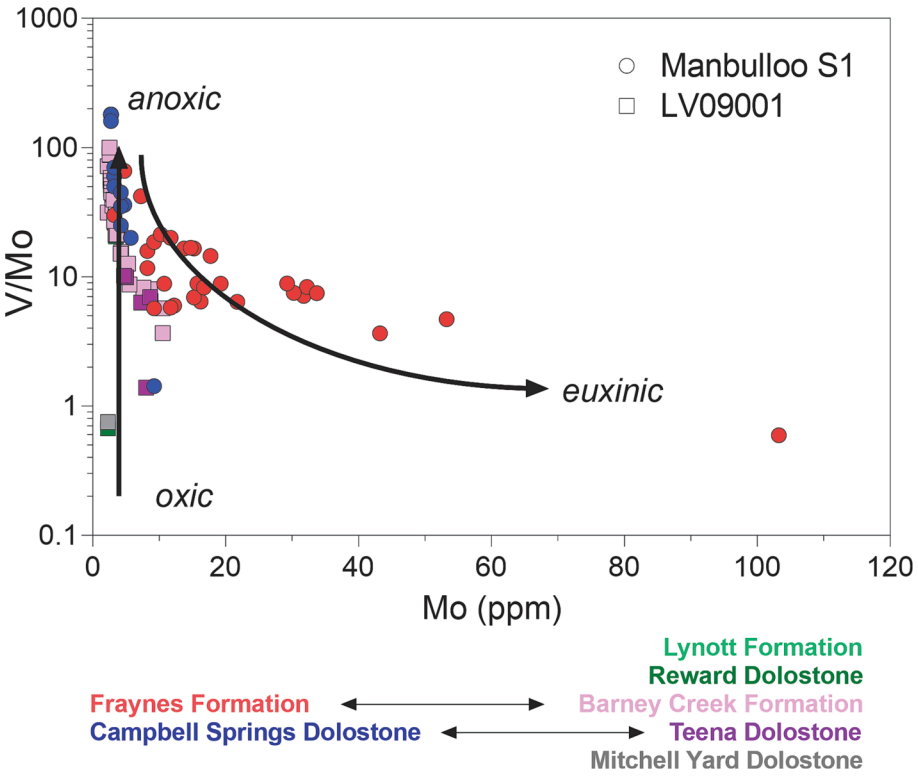

Fig. 6. V/Mo versus Mo palaeoredox plot showing the heterogeneous conditions evident in the Glyde Package. High V/Mo ratios with low concentrations of Mo indicate suboxic-to-anoxic environments whereas low V/Mo ratios with high concentrations of Mo highlight periods of euxinia (Piper and Calvert, 2009; Xu et al., 2012). Similar to Fig. 5, this plot also shows that the Fraynes Formation is more euxinic than the Barney Creek Formation.

Table 1
Summary of the palaeoredox geochemical results in this study.

Unit	TOC (wt. %)			Mo (ppm)			V (ppm)		
	Min.	*Mean*	*Max.*	*Min.*	*Mean*	*Max.*	*Min.*	*Mean*	*Max.*
Lynott Formation	0.13	0.19	0.25	0.48	0.50	0.51	0.05	17.65	26.57
Reward Dolostone	1.08	1.59	2.08	0.27	0.71	1.23	25.37	26.25	27.18
Barney Creek Formation	0.11	2.06	4.71	0.29	3.37	8.30	24.61	33.62	51.10
Fraynes Formation	0.04	2.09	8.39	1.00	18.77	101.00	30.00	147.33	250.00
Teena Dolostone	0.14	1.86	5.01	2.47	4.50	6.38	8.07	27.46	44.40
Campbell Springs Dolostone	0.19	1.52	2.63	0.50	1.63	7.00	10.0	71.88	90.0

gave ages and $^{87}Sr/^{86}Sr$ initial ratios (denoted as $^{87}Sr/^{86}Sr_I$) in good agreement with each other. Two samples from the Barney Creek Formation sourced from depths 463.60 and 469.50 m depths in the well LV09001 were dated at 1634 ± 59 ($^{87}Sr/^{86}Sr_I$: 0.702 ± 0.005) and 1635 ± 67 Ma ($^{87}Sr/^{86}Sr_I$: 0.705 ± 0.010), respectively (Fig. 4). Analysis of shales from the Fraynes Formation from depths 785.24 and 868.75 m in Manbulloo S1 (Fig. 4) yielded ages of 1630 ± 57 ($^{87}Sr/^{86}Sr_I$: 0.700 ± 0.010) and 1636 ± 42 Ma ($^{87}Sr/^{86}Sr_I$: 0.690 ± 0.010). Notably, these Rb–Sr ages are within error of the expected ages for each unit (Fig. 2), derived from dating tuff layers within the corresponding formations in other localities (Kositcin and Carson, 2017; Munson et al., 2020; Page et al., 2000; Page and Sweet, 1998). Furthermore, the $^{87}Sr/^{86}Sr$ initial ratios calculated from their respective isochrons (Fig. 4) also overlapped with the expected $^{87}Sr/^{86}Sr$ signature of Proterozoic seawater ~ 0.705 (Chen et al., 2022b; Kuznetsov et al., 2018; Shields and Veizer, 2002).

5. Discussion

5.1. Geochronological constraints on the Glyde Package

The Rb–Sr ages and isotopic fingerprints from shale samples here (Fig. 4) overlaps with their expected depositional ages (Kositcin and Carson, 2017; Munson et al., 2020; Page et al., 2000; Page and Sweet, 1998) as well as the coeval palaeowater $^{87}Sr/^{86}Sr$ chemistry (Chen et al., 2022b; Kuznetsov et al., 2018; Shields and Veizer, 2002). Consequently, these results are interpreted as minimum age constraints for the two respective units, recording an early diagenetic event in equilibrium with the surrounding formation waters during or soon after deposition (Subarkah et al., 2021). Importantly, these signatures show no evidence of disturbance by a late-stage alteration event (Subarkah et al., 2022). As such, they provide a conservative depositional window for the Barney Creek Formation and the Fraynes Formation, and directly correlate these distal units. It should be noted that these Rb–Sr shale ages have associated uncertainties that are orders of magnitude larger than the pre-existing U–Pb tuff ages (Kositcin and Carson, 2017; Munson et al., 2020; Page et al., 2000; Page and Sweet, 1998). However, tuff marker beds can be difficult to find in sedimentary basins. Consequently, this technique can still be a powerful tool to provide the depositional window of a sedimentary package where volcanic layers are unavailable but black shales are present.

These geochronological interpretations are further corroborated by high-resolution petrographic imagery of the samples (Supplementary Figure 4). Targeted clay phases are often mottled, filling gaps in pore spaces or between detrital grains. These morphologies have been

identified and similarly found elsewhere in the Proterozoic marine sedimentary rocks and were interpreted to be a product of reverse weathering processes (Deepak et al., 2022; Kennedy et al., 2006; Kennedy et al., 2002; Rafiei and Kennedy, 2019; Rafiei et al., 2020; Subarkah et al., 2021). In addition, early diagenetic sulfides often grow together with iron-carbonate minerals. This is often an important indicator of anoxic water columns with varying stability of sulfur (Mozley and Wersin, 1992). As such, they are further evidence that the samples analysed have not experienced extensive post-depositional alteration or metamorphism.

5.2. Water column palaeoredox conditions of the Glyde Package

The lack of post-depositional geochemical alteration (Fig. 3) means that the data can be used for palaeoenvironment investigations as well as correlating distal sequences. Samples here were analysed for several redox-sensitive trace elements to assess the oxygenation conditions of the formation waters during the deposition of the respective units. Different lithologies of marine sedimentary rocks have been used concurrently to reconstruct past water basin water chemistry and palaeoenvironments (Bauer et al., 2021; Chen et al., 2021; Farrell et al., 2021; Yano et al., 2020; Zhang and Shields, 2022). The two main palaeoredox proxies used in this study are enrichments in molybdenum (Mo) and vanadium (V). Mo is a commonly used trace element redox proxy as it is the most abundant trace metal in the modern ocean (Millero, 1996; Wright, 1995). In anoxic and relatively low H_2S conditions, Mo is enriched within the sediment as it forms thiomolybdates and preserves organo-metallic complexes (Helz et al., 1996; Vorlicek and Helz, 2002). In this threshold, Mo concentrations have a strong, positive relationship with total organic carbon (TOC) content (Fig. 5), indicating oxygen-poor water columns (Scott and Lyons, 2012). Above this threshold, increasingly euxinic environments do not necessarily generate higher Mo concentrations (Scott et al., 2017). Instead, Mo experiences hyper enrichment during euxinia when there is a significant reservoir of Mo in the seawater (Algeo and Maynard, 2004; Scott et al., 2008), where it can then be sequestered from the water column (Berrang and Grill, 1974; Morse and Luther III, 1999). In short, Mo concentrations of < 25 ppm can be interpreted as oxic-suboxic bottom waters, 25 ppm $<$ Mo < 100 ppm reflect an intermittently euxinic environment, and Mo > 100 ppm reflect a persistently euxinic water column (Scott et al., 2017). Similarly, V^{4+} also undergoes further reduction to V^{3+} by reactions with hydrogen sulphide (Wanty and Goldhaber, 1992). This relationship is similarly mirrored by abundance in V (Fig. 5). This is because in the presence of anoxia, V^{5+} is reduced to V^{4+} (Breit and Wanty, 1991). Hyper enrichment of V commonly occur between 2 and 4.5 wt% TOC (Scott et al., 2017).

The relationships between both elements and TOC content breaks down in euxinic water columns (Fig. 5), as sulphides become a competing sink for Mo and V against organic compounds (Algeo and Maynard, 2004; Tribovillard et al., 2006). Importantly, under oxic conditions, both elements will be deposited in the detrital phase, displaying no relationships with TOC content and are depleted in the sediment (Algeo and Maynard, 2004; Piper and Calvert, 2009; Tribovillard et al., 2006). The fact that V accumulates more readily under suboxic to anoxic conditions, relative to euxinic environments (Emerson and Huested, 1991; Wanty and Goldhaber, 1992) allows these two redox sensitive trace elements to be used together to distinguish complex bottom water heterogeneity (Fig. 6). Low V/Mo ratios are more reflective of euxinia, and in contrast, high V/Mo ratios suggests anoxic water columns (Piper and Calvert, 2009; Spinks et al., 2016a).

Trace element proxies in this study show that the Teena Dolostone from the McArthur Group and the Campbell Springs Dolostone from the Limbunya Group do not exhibit any significant relationships between TEs and TOC content (Fig. 5). As such, we suggest that these units were deposited beneath a relatively suboxic water column, likely between the Mn-oxide to Fe-oxide zone (Scott and Lyons, 2012). This is similarly indicated by the high V/Mo ratios (Fig. 6) of these units (Piper and Calvert, 2009). Further up stratigraphy, the Barney Creek Formation and the Fraynes Formation both displays a more complex redox history (Figs. 5 and 6). Here, V and Mo exhibits a strong, positive relationship with TOC content between 1 and 4 wt% (Fig. 5), indicating an anoxic system, and consistent with organic matter being the dominant sink for TEs (Algeo and Maynard, 2004; Scott and Lyons, 2012). Notably, this linear covariation breaks down above a TOC content of 4 wt%. At these elevated TOC values, V and Mo are even more enriched in the sediment as they are scavenged by precipitating sulfides during water column euxinia (Algeo and Maynard, 2004; Scott and Lyons, 2012). This threshold was similarly recorded in the Velkerri Formation, where bioproductivity have been suggested to drive redox-heterogeneity in the water column (Cox et al., 2022; Cox et al., 2016). However, the results from the Fraynes Formation suggests that it has experienced a more intense sulfidic environment in comparison to the Barney Creek Formation. Here, the relationship between redox-sensitive trace elements and TOC breaks down more readily, and the sediment is hyper-enriched in Mo (Figs. 5 and 6). Such conditions would make the Fraynes Formation highly prospective for hosting base-metal mineralisation as well as hydrocarbon resources; as euxinic sediments are excellent traps for metallogenic fluids and preserving organic matter (Calvert and Pedersen, 1993; Degens and Mopper, 1975; Demaison and Moore, 1980; Large and Wolf, 1981; Lyons et al., 2006; Spinks et al., 2016b; Walters, 2006). This euxinic period in the Fraynes Formation is further supported by the low V/Mo ratios with high Mo content (Fig. 6), implying that the unit experienced enrichment in Mo but not V (Piper and Calvert, 2009). Notably, Scott et al. (2017) have also suggest that sediments with Mo content between 25 and 100 ppm have experienced intermittent euxinia. Prior to the deposition of the Barney Creek Formation and the Fraynes Formation, the package seems be to relatively more oxygen-rich (Fig. 6). This transient period of oxia seems to be extensive, as correlative sections from the Teena Dolostone and the Campbell Springs Dolostone records similar signatures. Marine sediments with Mo < 25 ppm have been interpreted to be deposited under oxic to suboxic bottom waters (Scott et al., 2017). After the deposition of the Barney Creek Formation and the Fraynes Formation, the package transitioned back into relatively more oxygen-rich basin waters, reflected by the Reward Dolostone and the Lynott Formation (Fig. 6).

However, it is possible that this redox variability also occurs laterally, as the basin undergoes a change in palaeogeography and the same formations record different facies (Kunzmann et al., 2022). If this is true, the geochemical signatures here may not be totally representative of their respective units. Nevertheless, this redox heterogeneity hints at how complex this Proterozoic continental seaway was during its formation. Consequently, the delay of widespread anoxia or euxinia during here could be important for the survival of early biological life in this period (Spinks et al., 2016a).

5.3. Palaeoenvironment and tectonic evolution of the Glyde Package evidenced by isotopic excursions

The palaeoenvironment and tectonic evolution of the basin have been shown to be an important control on its coeval water chemistry (Benitez-Nelson, 2000; Calvert and Pedersen, 1993; Chen et al., 2022b; Condie et al., 2001; Derry and Jacobsen, 1988; El Meknassi et al., 2020; Tostevin et al., 2016). Such variability can be tracked by several isotopic proxies. For example, the $\delta^{13}C_{carb}$ isotope values of unaltered marine carbonates have been used to deduce the composition of the dissolved inorganic carbon (DIC) pool for its coeval water column (Knoll et al., 1986; Schidlowski, 1988). Biological activity plays a key role in the DIC reservoir, as processes like photosynthesis preferentially remove lighter ^{12}C from the water mass, resulting in the DIC pool being isotopically heavier (Kump and Arthur, 1999). In contrast, organic matter remineralisation can reintroduce ^{12}C into the water column, consequently leaving the DIC pool isotopically lighter (Sarmiento et al., 2007). As a

result, the changes in the $\delta^{13}C_{carb}$ record can fingerprint the interplay between these processes. Furthermore, cogenetic marine carbonates that precipitated distally can also retain the same $\delta^{13}C_{carb}$ excursions, as the residence time of C in oceans is orders of magnitude longer than the typical mixing time of seawater (Kump and Arthur, 1999; Shields and Veizer, 2002). As such, shifts in in $\delta^{13}C_{carb}$ can be applied for chemostratigraphic studies in local, regional, and global scale (Hayes and Waldbauer, 2006; Shields-Zhou and Mills, 2017; Shields and Veizer, 2002; Veizer et al., 1999; Veizer et al., 1992).

In addition to the $\delta^{13}C_{carb}$ isotope excursions, the Sr composition of marine carbonates can also be used to unravel the evolution of the basin, and the relative inputs of marine versus continental Sr sources. In particular, the $^{87}Sr/^{86}Sr$ signatures from authigenic marine carbonates can reflect the provenance into the sedimentary system, relative input of Sr between hydrothermal/marine and riverine sources, as well as silicate weathering from continental erosion (Banner, 2004; Chen et al., 2022b; Derry and Jacobsen, 1988; El Meknassi et al., 2020; Kuznetsov et al., 2018; Veizer et al., 1999). Higher ratios in the global palaeoseawater $^{87}Sr/^{86}Sr$ archive reflect increased erosion of ancient rocks, often caused by an escalation in global mountain belt development that

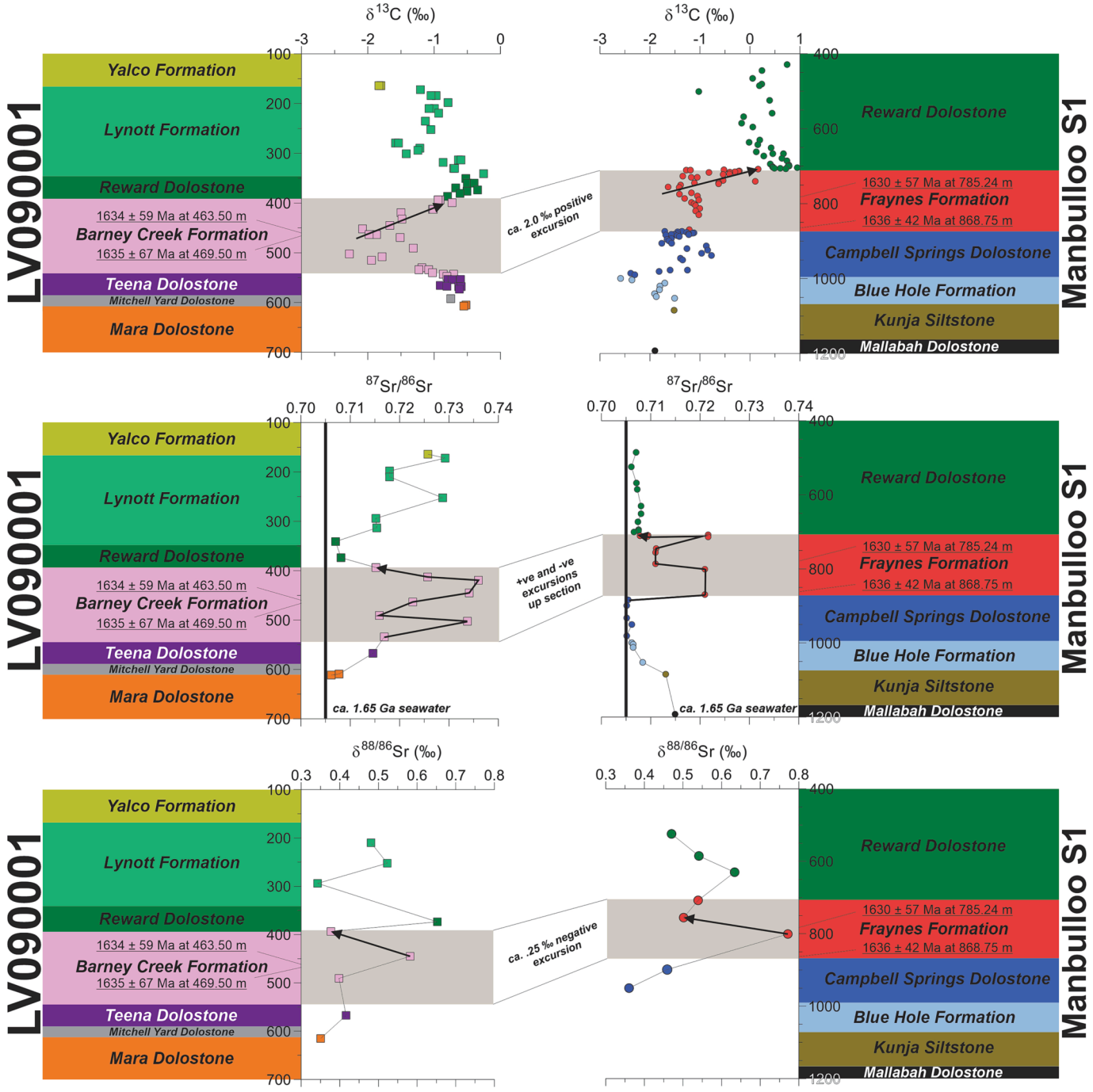

Fig. 7. Chemostratigraphic correlations between the McArthur Group sampled from LV09001 and the Limbunya Group from Manbulloo S1. Similar patterns in $\delta^{13}C_{carb}$, $^{87}Sr/^{86}Sr$, and $\delta^{88/86}Sr$ isotopic signatures from carbonate lithologies further suggests that the Barney Creek Formation and the Fraynes Formation are contemporaneous units. This includes a $\delta^{13}C_{carb}$ excursion of ~+2.0 ‰, a trend towards lower $^{87}Sr/^{86}Sr$ ratios up-section, and a $\delta^{88/86}Sr$ excursion of ~-0.25 ‰ (relative to NIST987). These similarities also suggests that basin-scale evolution of the Glyde Package can be recorded by distal sequences in the McArthur Basin and the Birrindudu Basin.

appears to reflect supercontinent amalgamation and continent–continent collisions (Kuznetsov et al., 2018). Conversely, lower ratios can be driven by an influx of mantle/oceanic crust derived Sr from rift boundaries in relation to supercontinent break-up (Semikhatov et al., 2002). Furthermore, the presence of large igneous provinces and mantle plumes can also drive the $^{87}Sr/^{86}Sr$ values of palaeoseawater lower (Prokoph et al., 2004).

However, it should be noted that the changes in the palaeoseawater $^{87}Sr/^{86}Sr$ record do not track fluctuations linked to the carbonate cycle or the removal of Sr via deposition of carbonates (Krabbenhöft et al., 2010; Vollstaedt et al., 2014). The input and outputs of the ocean's Sr budget can instead be traced by mass-dependent fractionation processes of stable $\delta^{88/86}Sr$ through carbonate formation or dissolution (Andrews et al., 2016; Krabbenhöft et al., 2010; Shalev et al., 2017; Shao et al., 2021). During the precipitation of carbonates in marine settings, lighter Sr isotopes are preferentially removed from seawater into carbonate minerals, with an average $\delta^{88/86}Sr$ offset of −0.18‰ to −0.21‰ (Shao et al., 2021; Vollstaedt et al., 2014). As such, this mechanism drives the palaeoseawater stable Sr isotopic signature heavier. Additionally, igneous differentiation and continental weathering processes can also drive fractionation of stable Sr isotopes. The influx of Sr from detritus transported by rivers from continental weathering can induce slightly lighter $\delta^{88/86}Sr$ values but higher $^{87}Sr/^{86}Sr$ ratios (Amsellem et al., 2018; Charlier et al., 2012; Chen et al., 2022a; de Souza et al., 2010; Krabbenhöft et al., 2010; Vollstaedt et al., 2014). On the contrary, basins sourcing more mafic materials might exhibit slightly higher $\delta^{88/86}Sr$ values but lower $^{87}Sr/^{86}Sr$ ratios (Amsellem et al., 2018; Charlier et al., 2012).

The combination of these isotopic proxies can be used to investigate the evolution of the basin system across distal locations, as they would be less susceptible to localised changes such as sedimentation rate, accumulation, or preservation (Canfield, 1994; Ingall et al., 1993; Müller and Suess, 1979; Tyson, 2005). Fig. 7 shows that the bottom of the McArthur Group, in this study sampled from the Mara Dolostone, Mitchell Yard Dolostone, and the Teena Dolostone, all recorded a steady $\delta^{13}C_{carb}$ value of −1.0 ‰. This constancy is similarly reflected by the $\delta^{88/86}Sr$ results from this section, which hover at 0.35–0.4‰ (Fig. 7). However, the $^{87}Sr/^{86}Sr$ signatures here notably vary (Fig. 7), with a transition from palaeoseawater-like $^{87}Sr/^{86}Sr$ ratios (~0.705) in the Mara Dolostone to that more reflective of a restricted setting in the Teena Dolostone (Chen et al., 2022b; El Meknassi et al., 2020). Notably, these trends are similarly shown by the Campbell Springs Dolostone in the Limbunya Group (Fig. 7). The chemostratigraphic evidence here, along with correlations in lithostratigraphy (Cutovinos et al., 2002; Dunster, 1998; Sweet et al., 1974) and geochronology (Cutovinos et al., 2002; Page et al., 2000) further corroborates that they are coeval units. Consequently, these results may indicate that the DIC reservoir and the carbonate precipitation/dissolution mechanism remains relatively constant during the deposition of these formations. On the other hand, the sedimentary system seems to evolve and become progressively more restricted. The analogous palaeoenvironments recorded in these formations could explain why they recorded similar palaeoredox conditions (Figs. 5 and 6).

Further up stratigraphy, the Barney Creek Formation and the Fraynes Formation continue to mirror the changes in isotope geochemistry. Both these formations preserve a $\delta^{13}C_{carb}$ excursion of ca. + 2.0 ‰, with an initial trend towards higher $^{87}Sr/^{86}Sr$ ratios followed by lower values at the top, and a negative $\delta^{88/86}Sr$ −0.25 ‰ shift. This complex period is also reflected in the heterogeneous redox history of these units, as both formations fluctuate between euxinic-to-sub-oxic conditions (Figs. 5 and 6). Here, heavier $\delta^{13}C_{carb}$ values at the termination of the Barney Creek Formation and the Fraynes Formation coincide with lower $^{87}Sr/^{86}Sr$ ratios and lighter $\delta^{88/86}Sr$ results (Fig. 7). Such relationships suggest that biological productivity thrived better as the restricted basin reconnected to more marine waters. These trends may be induced by the introduction of more nutrient-rich, oxic waters or up-welling zones flooding a previously restricted palaeoenvironment (Condie et al., 2001; Piper and Perkins, 2004; Shen et al., 2000; Tyson and Pearson, 1991). These intermittent periods of basin connectivity and restriction would also have had a profound effect on salinity and carbonate saturation, subsequently controlling the precipitation and dissolution of $CaCO_3$ (Diloreto et al., 2021; Shao et al., 2021).

The McArthur Basin and the Birrindudu Basin continue to display analogous geochemical results after the deposition of the previous units. Here, the Reward Dolostone is recorded in both boreholes LV090001 (Schmid, 2015) and Manbulloo S1 (NTGS., 2015), with both yielding a $\delta^{13}C_{carb}$ values of −0.5 ‰, and $^{87}Sr/^{86}Sr$ ratios close to palaeoseawater (Chen et al., 2022b). Although these results are comparable to the older Mara Dolostone and their equivalents (Fig. 7), the Reward Dolostone noticeably gave a much heavier $\delta^{88/86}Sr$ signature of ca. 0.6 ‰. This discrepancy could be explained by differences in the local rate of carbonate deposition (Krabbenhöft et al., 2010; Vollstaedt et al., 2014), as hypersaturation of $CaCO_3$ in basin waters is expected to be reflected as an increasing trend of $\delta^{88/86}Sr$ (Shao et al., 2021). The Lynott Formation and the Yalco Formation in the McArthur Basin have no proposed correlative sequences in the Birrindudu Basin (Ahmad and Munson, 2013; Munson, 2019; Page et al., 2000). However, these units revert back to a more restricted setting, reflected by higher $^{87}Sr/^{86}Sr$ ratios (Fig. 7). This interpretation is further supported by the shift into lower $\delta^{88/86}Sr$ ratios, which suggests an increase in flux of continent-derived Sr into the semi-restricted environment (Amsellem et al., 2018; Charlier et al., 2012; Krabbenhöft et al., 2010; Paytan et al., 2021; Vollstaedt et al., 2014). These sources would be relatively nutrient-poor, and consequently inhibits biological activity. This delimiting factor looks to be recorded by further negative excursions in $\delta^{13}C_{carb}$ of the units.

5.4. Implications for exploration

The geochemical and geochronological findings from this study demonstrates correlations between the Zn-Pb hosting Barney Creek Formation in the McArthur Basin with the Fraynes Formation in the Birrindudu Basin. Ore genesis models for the McArthur River HYC mineralisation suggests that metals were transported by oxidising, sulfide-poor fluids and consequently precipitated in a reducing and sulfidic layer (Cooke et al., 2000; Huston et al., 2016; Huston et al., 2006; Large et al., 1998). If this is true, the Fraynes Formation would be an excellent redox gradient to trap metal-bearing fluids as it is readily abundant in organic matter (Fig. 5). In this case study, the Fraynes Formation records even more sulfidic water column chemistry than the Barney Creek Formation (Figs. 5 and 6) and potentially would be a better chemical trap if mineralisation was driven by a sedimentary exhalative process (Large and Wolf, 1981; Large et al., 1998). On the other hand, an excessively euxinic environment may not be optimal for base-metal mineralisation. Brines that are too rich in H_2S cannot transport Zn at lower temperatures (Cooke et al., 2000; Huston et al., 2006). As such, the Fraynes Formation might be a good chemical trap for precipitating metals but not conducive for transporting them. The potential for both units to be targets for base-metal mineralisation induced by sedimentary exhalative brines may also be recorded in their Sr isotope signatures. Sedimentary exhalative brines may be able to cause spikes in the marine $^{87}Sr/^{86}Sr$ record by introducing radiogenic Sr-rich fluids and generating positive excursions for a short duration (Emsbo, 2017). Positive and negative excursions up stratigraphy are recorded in both the Barney Creek Formation and the Fraynes Formation here (Fig. 7).

However, recent studies based on high-resolution geochemical mapping of ore samples from the HYC deposit suggest that mineralisation occurs as a diagenetic product exclusively associated with carbonate dissolution (Spinks et al., 2021). In this interpretation, metallogenic fluids are introduced post-depositionally. The bituminous black shales of the Barney Creek Formation (or the Fraynes Formation) would already be lithified, acting as a physical barrier instead of a chemical one

(Kunzmann et al., 2019; Spinks et al., 2021). In this case, the fine-grained, impermeable, black shale would serve as a seal, physically trapping metalliferous brines migrating through faults, with mineralisation occurring underneath in more unlithified sediments and forming as a product of carbonate replacement (Kunzmann et al., 2019; Spinks et al., 2021). Nevertheless, the trapping potential of the Barney Creek Formation and their equivalents is only one component of the mineral system and other variables to the mineralisation paragenesis must be considered.

6. Conclusions

The *in situ* Rb–Sr dating of Barney Creek Formation and Fraynes Formation shales in this study provides the depositional window of these units and directly correlates them (Fig. 4). In addition, several isotopic proxies such as $\delta^{13}C_{carb,}$ $^{87}Sr/^{86}Sr$, and $\delta^{88/86}Sr$ show that the basin's tectonic regime plays a critical part in what detritus or nutrient flux is being sourced into the system (Fig. 7). In turn, these processes are the main driver of bioproductivity and redox conditions (Figs. 5 and 6) in the palaeowaters (Anbar and Knoll, 2002; Cox et al., 2016; Dessert et al., 2003; Horton, 2015; Yang et al., 2020). This approach of combining sedimentology and sedimentary geochemistry is proving an ideal combination to better understand these often enigmatic Proterozoic basins (Virgo et al., 2021) The heterogeneity in oxygenation conditions indicated by redox-sensitive trace elements V and Mo relate to the changing palaeoenvironments, and are integral in forming potential source rocks for base-metal mineralisation and hydrocarbon reservoirs (Calvert and Pedersen, 1993; Degens and Mopper, 1975; Demaison and Moore, 1980; Large and Wolf, 1981; Lyons et al., 2006; Spinks et al., 2016b; Walters, 2006). Importantly, our study shows that the complex basin evolution of the Glyde Package is extensively recorded in the distal sequences of the McArthur Basin and the Birrindudu Basin. As such, the Birrindudu Basin may also be primed for hosting similar economic targets that are present in the McArthur Basin.

Declaration of Competing Interest

The authors declare that they have no known competing financial interests or personal relationships that could have appeared to influence the work reported in this paper.

Data availability

Data from this work is attached as a file in the submission of this manuscript.

Acknowledgements

This work was supported by the Australian Research Council Projects LP160101353 and LP200301457 in collaboration with Santos Ltd, Empire Energy Group Ltd, Northern Territory Geological Survey, Teck Resources, BHP, and Origin as partners. The initial development and validation of *in situ* Rb–Sr dating technique at the University of Adelaide was also supported by Agilent Technologies Australia Ltd. This manuscript forms MinEx CRC contribution #2023/30. Aoife McFadden is thanked for their assistance in the SEM mapping of the samples in this study. Robert Klaebe and Yuexiao Shao are thanked for their support in the laboratory analysis. Jarred Lloyd is thanked for his help in the laser data processing. Jarred Lloyd's code to process error correlations on LADR can be found in https://github.com/jarredclloyd/PowerShell_LADR_errorcorrelation_workaround.

Appendix A. Supplementary data

Supplementary data to this article can be found online at https://doi.org/10.1016/j.oregeorev.2023.105499.

References

Ahmad, A., Munson, T.J., 2013. Geology and mineral resources of the Northern Territory. Special Publication, Northern Territory Geological Survey.
Algeo, T.J., Maynard, J.B., 2004. Trace-element behavior and redox facies in core shales of Upper Pennsylvanian Kansas-type cyclothems. Chemical Geology 206 (3), 289–318.
Allan, J.R., Matthews, R.K., 1982. Isotope signatures associated with early meteoric diagenesis. Sedimentology 29 (6), 797–817.
Amsellem, E., Moynier, F., Day, J.M.D., Moreira, M., Puchtel, I.S., Teng, F.-Z., 2018. The stable strontium isotopic composition of ocean island basalts, mid-ocean ridge basalts, and komatiites. Chemical Geology 483, 595–602.
Anbar, A.D., Knoll, A.H., 2002. Proterozoic ocean chemistry and evolution: a bioinorganic bridge? Science 297 (5584), 1137–1142.
Andrews, M.G., Jacobson, A.D., Lehn, G.O., Horton, T.W., Craw, D., 2016. Radiogenic and stable Sr isotope ratios (87Sr/86Sr, δ88/86Sr) as tracers of riverine cation sources and biogeochemical cycling in the Milford Sound region of Fiordland. New Zealand: Geochimica et Cosmochimica Acta 173, 284–303.
S.E. Armistead A.S. Collins A. Redaa G. Jepson J. Gillespie S. Gilbert M.L. Blades J.D. Foden T. Razakamanana Structural evolution and medium-temperature thermochronology of central Madagascar: implications for Gondwana amalgamation Journal of the Geological Society 2020 p. jgs2019-2132.
Balcaen, L., Schrijver, I.D., Moens, L., Vanhaecke, F., 2005. Determination of the 87Sr/86Sr isotope ratio in USGS silicate reference materials by multi-collector ICP–mass spectrometry. International Journal of Mass Spectrometry 242 (2), 251–255.
Banner, J.L., 2004. Radiogenic isotopes: systematics and applications to earth surface processes and chemical stratigraphy. Earth-Science Reviews 65 (3), 141–194.
Banner, J., Hanson, G., 1990. Calculation of simultaneous isotopic and trace element variations during water-rock interaction with applications to carbonate diagenesis. Geochimica et Cosmochimica Acta 54, 3123–3137.
Bauer, K.W., Planavsky, N.J., Reinhard, C.T., Cole, D.B., 2021. The Chromium Isotope System as a Tracer of Ocean and Atmosphere Redox: Cambridge. Cambridge University Press.
Benitez-Nelson, C.R., 2000. The biogeochemical cycling of phosphorus in marine systems. Earth-Science Reviews 51 (1–4), 109–135.
Berrang, P., Grill, E., 1974. The effect of manganese oxide scavenging on molybdenum in Saanich Inlet. British Columbia: Marine Chemistry 2 (2), 125–148.
Blaikie, T., and Kunzmann, M., 2017, Towards an improved understanding of the 3D structural architecture of the greater McArthur Basin through geophysical interpretation and modelling, in Annual Geoscience Exploration Seminar Proceedings, Alice Springs, 28 March 2017, Northern Territory Geological Survey, p. 112. https://geoscience.nt.gov.au/gemis/ntgsjspui/handle/1/85111.
Blaikie, T., and Kunzmann, M., 2019, Sub-basin architecture of the Proterozoic McArthur Group, southern McArthur Basin: ASEG Extended Abstracts, v. 2019, no. 1, p. 1-4.
Blaikie, T. N., and Kunzmann, M., 2020, Geophysical interpretation and tectonic synthesis of the Proterozoic southern McArthur Basin, northern Australia: Precambrian Research, v. 343, p. 105728.
Bodorkos, S., Crowley, J.L., Claoué-Long, J.C., Anderson, J.R., Magee, C.W., 2022. Precise U-Pb baddeleyite dating of the Derim Derim Dolerite, McArthur Basin, Northern Territory: old and new SHRIMP and ID-TIMS constraints. Australian Journal of Earth Sciences 1–15.
Bradshaw, M.T., Bradshaw, J., Murray, A., Needham, J., Spencer, L., Summons, R.E., Wilmot, J., S., W., 1994. Petroleum Systems in West Australian Basins. *In*: Purcell, P. G., Purcell, R.R. (Eds.), The Sedimentary Basins of Western Australia: Proceedings of the Petroleum Exploration Society of Australia, pp. 93–118 (Perth, 1994). https://archives.datapages.com/data/petroleum-exploration-society-of-australia/conferences/012/012001/pdfs/93.html.
Breit, G.N., Wanty, R.B., 1991. Vanadium accumulation in carbonaceous rocks: A review of geochemical controls during deposition and diagenesis. Chemical Geology 91 (2), 83–97.
Brocks, J.J., Love, G.D., Summons, R.E., Knoll, A.H., Logan, G.A., Bowden, S.A., 2005. Biomarker evidence for green and purple sulphur bacteria in a stratified Palaeoproterozoic sea. Nature 437 (7060), 866–870.
Bruisten, B., and Brocks, J. J., 2015, Organic and inorganic geochemical analyses of the Barney Creek Formation, McArthur Basin, Australia: Australian National University, CSR0265.
Bull, S., 1998. Sedimentology of the Palaeoproterozoic Barney Creek Formation in DDH BMR McArthur 2, southern McArthur basin, northern territory. Australian Journal of Earth Sciences 45 (1), 21–31.
Calvert, S.E., Pedersen, T.F., 1993. Geochemistry of Recent oxic and anoxic marine sediments: Implications for the geological record. Marine Geology 113 (1), 67–88.
Canfield, D.E., 1994. Factors influencing organic carbon preservation in marine sediments: Chemical geology 114 (3–4), 315–329.
B.L.A. Charlier G.M. Nowell I.J. Parkinson S.P. Kelley D.G. Pearson K.W. Burton High temperature strontium stable isotope behaviour in the early solar system and planetary bodies Earth and Planetary Science Letters v 2012 329–330, p. 31–40.
Chen, X., Tissot, F.L.H., Jansen, M.F., Bekker, A., Liu, C.X., Nie, N.X., Halverson, G.P., Veizer, J., Dauphas, N., 2021. The uranium isotopic record of shales and carbonates through geologic time. Geochimica et Cosmochimica Acta 300, 164–191.
Chen, X.-Q., Zeng, Z., Yu, H.-M., Sun, N., Huang, F., 2022a. Precise measurements of δ88/86Sr for twenty geological reference materials by double-spike MC-ICP-MS. International Journal of Mass Spectrometry 479, 116883.
Chen, X., Zhou, Y., Shields, G.A., 2022b. Progress towards an improved Precambrian seawater 87Sr/86Sr curve. Earth-Science Reviews 224, 103869.

Close, D., 2014. The McArthur Basin: NTGS' approach to a frontier petroleum basin with known base metal prospectivity. Annual Geoscience Exploration Seminar Alice Springs, Northern Territory Geological Survey.

A. Collins J. Farkas S. Glorie M. Blades G. Cox J. Foden T. Hall J. Payne B. Yang A. Nixon Life and times of the Proterozoic McArthur-Yanliao Gulf: Update on the ARC-Industry-NTGS Linkage Project 2019.

Condie, K.C., Des Marais, D.J., Abbott, D., 2001. Precambrian superplumes and supercontinents: a record in black shales, carbon isotopes, and paleoclimates? Precambrian Research 106 (3–4), 239–260.

Cooke, D.R., Bull, S.W., Large, R.R., McGoldrick, P.J., 2000. The importance of oxidized brines for the formation of Australian Proterozoic stratiform sediment-hosted Pb-Zn (Sedex) deposits. Economic Geology 95 (1), 1–18.

Cox, G. M., Collins, A. S., Jarrett, A. J., Blades, M. L., Shannon, A. V., Yang, B., Farkas, J., Hall, P. A., O'Hara, B., and Close, D. J. A. B., 2022, A very unconventional hydrocarbon play: the Mesoproterozoic Velkerri Formation of northern Australia, no. 20,220,110.

Cox, G.M., Jarrett, A., Edwards, D., Crockford, P.W., Halverson, G.P., Collins, A.S., Poirier, A., Li, Z.-X., 2016. Basin redox and primary productivity within the Mesoproterozoic Roper Seaway. Chemical Geology 440, 101–114.

Cox, G.M., Sansjofre, P., Blades, M.L., Farkas, J., Collins, A.S., 2019. Dynamic interaction between basin redox and the biogeochemical nitrogen cycle in an unconventional Proterozoic petroleum system. Sci Rep 9 (1), 5200.

Craig, J., Biffi, U., Galimberti, R., Ghori, K., Gorter, J., Hakhoo, N., Le Heron, D., Thurow, J., Vecoli, M., 2013. The palaeobiology and geochemistry of Precambrian hydrocarbon source rocks. Marine and Petroleum Geology 40, 1–47.

Crick, I., Boreham, C., Cook, A., Powell, T., 1988. Petroleum geology and geochemistry of Middle Proterozoic McArthur Basin, northern Australia II: Assessment of source rock potential. AAPG bulletin 72 (12), 1495–1514.

Croon, M., Bluett, J., Titus, L., Johnson, R., 2015. Formation evaluation case study: Glyde unconventional Middle Proterozoic play in the McArthur Basin, northern Australia. The APPEA Journal 55 (2), 429.

Croxford, N., Gulson, B., Smith, J., 1975. The McArthur deposit: A review of the current situation. Mineralium Deposita 10 (4), 302–304.

Cutovinos, A., Beier, P., Kruse, P., Abbott, S., Dunster, J., Brescianini, R., Abbot, S., Dunster, J., and Brescianini, R., 2002, Limbunya, Northern Territory , 1: 250 000 geological map series and explanatory notes, SE 52-07: Northern Territory Geological Survey, Darwin and Alice Springs.

Deepak, A., Löhr, S., Abbott, A. N., Han, S., Wheeler, C., and Sharma, M., 2022, Testing the Precambrian reverse weathering hypothesis using a 1-billion-year record of marine shales, in Proceedings Goldschmidt Conference, Honolulu, Hawai'i', USA, 12 July 2022, Goldschmidt. https://conf.goldschmidt.info/goldschmidt/2022/meetingapp.cgi/Paper/10825.

de Souza, G.F., Reynolds, B.C., Kiczka, M., Bourdon, B., 2010. Evidence for mass-dependent isotopic fractionation of strontium in a glaciated granitic watershed. Geochimica et Cosmochimica Acta 74 (9), 2596–2614.

Debacker, T., Connors, K., Pryer, L., Blevin, J., Henley, P., and Shi, Z., 2021, The Northern Territory SEEBASE®: An updated, Territory-wide depth-to-basement model for explorers.

Degens, E.T., Epstein, S., 1962. Relationship between O18/O16 ratios in coexisting carbonates, cherts, and diatomites. AAPG Bulletin 46 (4), 534–542.

Degens, E., Mopper, K., 1975. Factors Controlling the Distribution and Early Diagenesis. Chemical oceanography 6, 59.

Demaison, G.J., Moore, G.T., 1980. Anoxic Environments and Oil Source Bed Genesis1. AAPG Bulletin 64 (8), 1179–1209.

Derkowski, A., Środoń, J., Franus, W., Uhlík, P., Banaś, M., Zieliński, G., Čaplovičová, M., Franus, M., 2009. Partial dissolution of glauconitic samples: Implications for the methodology of K-Ar and Rb-Sr dating. Clays and Clay Minerals 57 (5), 531–554.

Derry, L.A., Jacobsen, S.B., 1988. The Nd and Sr isotopic evolution of Proterozoic seawater. Geophysical Research Letters 15 (4), 397–400.

Dessert, C., Dupré, B., Gaillardet, J., François, L.M., Allegre, C.J., 2003. Basalt weathering laws and the impact of basalt weathering on the global carbon cycle. Chemical Geology 202 (3–4), 257–273.

Diloreto, Z.A., Garg, S., Bontognali, T.R.R., Dittrich, M., 2021. Modern dolomite formation caused by seasonal cycling of oxygenic phototrophs and anoxygenic phototrophs in a hypersaline sabkha. Scientific Reports 11 (1), 4170.

Ding, J., Shi, Y., Kröner, A., Anderson, J., 2017. Constraints on sedimentary ages of the Chuanlinggou Formation in the Ming Tombs, Beijing, North China Craton: LA-ICP-MS and SHRIMP U-Pb dating of detrital zircons: Acta. Geochimica 37, 1–24.

Dunster, J., 1998. Reconnaissance of the Proterozoic rocks of the. Northern Territory Geological Survey, Victoria River Region.

El Meknassi, S., Dera, G., De Rafélis, M., Brahmi, C., Lartaud, F., Hodel, F., Jeandel, C., Menjot, L., Mounic, S., Henry, M., Besson, P., Chavagnac, V., 2020. Seawater 87Sr/86Sr ratios along continental margins: Patterns and processes in open and restricted shelf domains. Chemical Geology 558, 119874.

Eldridge, C. S., Williams, N., and Walshe, J. L., 1993, Sulfur isotope variability in sediment-hosted massive sulfide deposits as determined using the ion microprobe SHRIMP; II, A study of the H.Y.C. Deposit at McArthur River, Northern Territory, Australia: Economic Geology, v. 88, no. 1, p. 1-26.

Emerson, S.R., Huested, S.S., 1991. Ocean anoxia and the concentrations of molybdenum and vanadium in seawater. Marine Chemistry 34 (3–4), 177–196.

Emsbo, P., 2017. Sedex brine expulsions to Paleozoic basins may have changed global marine 87Sr/86Sr values, triggered anoxia, and initiated mass extinctions. Ore Geology Reviews 86, 474–486.

Fanning, C., 1991. Ion microprobe U-Pb zircon dating of a tuffaceous horizon within the Kunja Siltstone, Victoria River Basin, Northern Territory. Research School of Earth Sciences, Australian National University, Report for Pacific Oil and Gas Pty Ltd, Canberra, ACT.

Farrell, Ú.C., Samawi, R., Anjanappa, S., Klykov, R., Adeboye, O.O., Agic, H., Ahm, A.-S.-C., Boag, T.H., Bowyer, F., Brocks, J.J., Brunoir, T.N., Canfield, D.E., Chen, X., Cheng, M., Clarkson, M.O., Cole, D.B., Cordie, D.R., Crockford, P.W., Cui, H., Dahl, T.W., Mouro, L.D., Dewing, K., Dornbos, S.Q., Drabon, N., Dumoulin, J.A., Emmings, J.F., Endriga, C.R., Fraser, T.A., Gaines, R.R., Gaschnig, R.M., Gibson, T. M., Gilleaudeau, G.J., Gill, B.C., Goldberg, K., Guilbaud, R., Halverson, G.P., Hammarlund, E.U., Hantsoo, K.G., Henderson, M.A., Hodgskiss, M.S.W., Horner, T. J., Husson, J.M., Johnson, B., Kabanov, P., Brenhin Keller, C., Kimmig, J., Kipp, M. A., Knoll, A.H., Kreitsmann, T., Kunzmann, M., Kurzweil, F., LeRoy, M.A., Li, C., Lipp, A.G., Loydell, D.K., Lu, X., Macdonald, F.A., Magnall, J.M., Mänd, K., Mehra, A., Melchin, M.J., Miller, A.J., Mills, N.T., Mwinde, C.N., O'Connell, B., Och, L.M., Ossa Ossa, F., Pagès, A., Paiste, K., Partin, C.A., Peters, S.E., Petrov, P., Playter, T.L., Plaza-Torres, S., Porter, S.M., Poulton, S.W., Pruss, S.B., Richoz, S., Ritzer, S.R., Rooney, A.D., Sahoo, S.K., Schoepfer, S.D., Sclafani, J.A., Shen, Y., Shorttle, O., Slotznick, S.P., Smith, E.F., Spinks, S., Stockey, R.G., Strauss, J.V., Stüeken, E.E., Tecklenburg, S., Thomson, D., Tosca, N.J., Uhlein, G.J., Vizcaíno, M. N., Wang, H., White, T., Wilby, P.R., Woltz, C.R., et al., 2021. The Sedimentary Geochemistry and Paleoenvironments Project: Geobiology 19 (6), 545–556.

French, K.L., Birdwell, J.E., Berg, M.V., 2020. Biomarker similarities between the saline lacustrine eocene green river and the paleoproterozoic barney creek formations. Geochimica et Cosmochimica Acta 274, 228–245.

Frogtech Geoscience, N. T. G. S., Digital Information Package, DIP, 2018, SEEBASE® study and GIS for greater McArthur Basin, v. 17.

Gianfriddo, C., Bull, S.W., Andrews, T.M., 2022. The Rosie pyrite hydrothermal system in the McArthur Basin: tectono-sedimentary constraints on mineralization and alkali metasomatism in stratiform sediment-hosted sulfide deposits of northern Australia. Mineralium Deposita 57 (3), 377–398.

Gibson, G.M., Hutton, L.J., Holzschuh, J., 2017. Basin inversion and supercontinent assembly as drivers of sediment-hosted Pb–Zn mineralization in the Mount Isa region, northern Australia. Journal of the Geological Society 174 (4), 773–786.

Gibson, G.M., Champion, D.C., Withnall, I.W., Neumann, N.L., Hutton, L.J., 2018. Assembly and breakup of the Nuna supercontinent: Geodynamic constraints from 1800 to 1600 Ma sedimentary basins and basaltic magmatism in northern Australia. Precambrian Research 313, 148–169.

Goodarzi, F., Gentzis, T., Sanei, H., Pedersen, P.K., 2019. Elemental Composition and Organic Petrology of a Lower Carboniferous-Age Freshwater Oil Shale in Nova 4, 20773–20786.

Govindaraju, K., Rubeska, I., Paukert, T., 1994. Report On Zinnwaldite Zw-C Analysed By Ninety-Two Git-Iwg Member-Laboratories. Geostandards Newsletter 18 (1), 1–42.

Gu, X., Zhang, Y., Schulz, O., Vavtar, F., Liu, J., Zheng, M., Zheng, L., 2012. The Woxi W-Sb–Au deposit in Hunan, South China: an example of late Proterozoic sedimentary exhalative (SEDEX) mineralization. Journal of Asian Earth Sciences 57, 54–75.

Gustafson, L. B., and Williams, N., 1981, Sediment-hosted stratiform deposits of copper, lead, and zinc.

Haines, P., The Balma and Habgood groups, northern McArthur Basin, Northern Territory; stratigraphy and correlations with the McArthur Group, *in* Proceedings 1994 AusIMM Annual Conference, Australian Mining Looks North; the Challenges and Choices1994, p. 147-152.

Hall, L., Boreham, C. J., Edwards, D. S., Palu, T., Buckler, T., Troup, A., and Hill, A., 2016, Cooper Basin Source Rock Geochemistry, Geoscience Australia.

Hamilton, M.A., Buchan, K.L., 2010. U-Pb geochronology of the Western Channel Diabase, northwestern Laurentia: implications for a large 1.59 Ga magmatic province, Laurentia's APWP and paleocontinental reconstructions of Laurentia, Baltica and Gawler craton of southern Australia. Precambrian Research 183 (3), 463–473.

Hayes, J.M., Waldbauer, J.R., 2006. The carbon cycle and associated redox processes through time. Philos Trans R Soc Lond B Biol Sci 361 (1470), 931–950.

Helz, G., Miller, C., Charnock, J., Mosselmans, J., Pattrick, R., Garner, C., Vaughan, D., 1996. Mechanism of molybdenum removal from the sea and its concentration in black shales: EXAFS evidence. Geochimica et Cosmochimica Acta 60 (19), 3631–3642.

Hoffman, T., 2014, New insights into the expanse of the McArthur Superbasin.

Hogmalm, K.J., Zack, T., Karlsson, A.K.O., Sjöqvist, A.S.L., Garbe-Schönberg, D., 2017. In situ Rb–Sr and K-Ca dating by LA-ICP-MS/MS: an evaluation of N2O and SF6 as reaction gases. Journal of Analytical Atomic Spectrometry 32 (2), 305–313.

Horton, F., 2015. Did phosphorus derived from the weathering of large igneous provinces fertilize the Neoproterozoic ocean?: Geochemistry. Geophysics, Geosystems 16 (6), 1723–1738.

Huston, D.L., Stevens, B., Southgate, P.N., Muhling, P., Wyborn, L., 2006. Australian Zn-Pb-Ag ore-forming systems: a review and analysis. Economic Geology 101 (6), 1117–1157.

Huston, D.L., Mernagh, T.P., Hagemann, S.G., Doublier, M.P., Fiorentini, M., Champion, D.C., Jaques, A.L., Czarnota, K., Cayley, R., Skirrow, R., 2016. Tectono-metallogenic systems—The place of mineral systems within tectonic evolution, with an emphasis on Australian examples. Ore Geology Reviews 76, 168–210.

Ingall, E.D., Bustin, R., Van Cappellen, P., 1993. Influence of water column anoxia on the burial and preservation of carbon and phosphorus in marine shales. Geochimica et Cosmochimica Acta 57 (2), 303–316.

Jackson, M.J., Powell, T.G., Summons, R.E., Sweet, I.P., 1986. Hydrocarbon shows and petroleum source rocks in sediments as old as 1.7 × 109 years. Nature 322 (6081), 727–729.

Jackson, M.J., Muir, M.D., Plumb, K.A., 1987. Geology of the Southern McArthur Basin. Australian Government Public Service, Northern Territory.

Jackson, J., Sweet, I.P., Powell, T.G., 1988. Studies On Petroleum Geology And Geochemistry. Middle Proterozoic, Mcarthur Basin Northern Australia I: Petroleum Potential: The APPEA Journal 28 (1), 283–302.
Jarrett, A.J., Cox, G.M., Brocks, J.J., Grosjean, E., Boreham, C.J., Edwards, D.S., 2019. Microbial assemblage and palaeoenvironmental reconstruction of the 1.38 Ga Velkerri Formation, McArthur Basin 17, 360–380.
Jarrett, A.J., Bailey, A., Chen, J., Munson, T.J., 2021. Petroleum geology and geochemistry of the Birrindudu Basin, greater McArthur Basin, *in* Proceedings Annual Geoscience Exploration Seminar (AGES) Proceedings. Northern Territory, Alice Springs, pp. 20–21.
A. Jarrett J. Chen Z. Hong G. Australia Birrindudu Basin TOC and Rock-Eval data release 2018 Australia, Northern Territory Geological Survey.
Jarrett, A.J.M., Munson, T.J., Williams, B., Bailey, A.H.E., Palu, T., 2022. Petroleum supersystems in the greater McArthur Basin. Northern Territory, Australia: prospectivity of the world's oldest stacked systems with emphasis on the McArthur Supersystem: The APPEA Journal 62, 245–262.
Jarvie, D., Breyer, J., 2011. Shale resource systems for oil and gas: Part 1–Shale gas resource systems; Part 2–Shale oil resource systems: Shale reservoirs–Giant resources for the 21st century. AAPG Memoir 97, 1–31.
Jegal, Y., Zimmermann, C., Reisberg, L., Yeghicheyan, D., Cloquet, C., Peiffert, C., Gerardin, M., Deloule, E., Mercadier, J., 2022. Characterisation of Reference Materials for In Situ Rb-Sr Dating by LA-ICP-MS/MS. Geostandards and Geoanalytical Research v. n/a, no. n/a.
Jochum, K.P., Willbold, M., Raczek, I., Stoll, B., Herwig, K., 2005. Chemical Characterisation of the USGS Reference Glasses GSA-1G, GSC-1G, GSD-1G, GSE-1G, BCR-2G, BHVO-2G and BIR-1G Using EPMA. ID-TIMS, ID-ICP-MS and LA-ICP-MS: Geostandards and Geoanalytical Research 29 (3), 285–302.
Jochum, K.P., Weis, U., Schwager, B., Stoll, B., Wilson, S.A., Haug, G.H., Andreae, M.O., Enzweiler, J., 2016. Reference Values Following ISO Guidelines for Frequently Requested Rock Reference Materials. Geostandards and Geoanalytical Research 40 (3), 333–350.
Johnston, D.T., Farquhar, J., Summons, R.E., Shen, Y., Kaufman, A.J., Masterson, A.L., Canfield, D.E., 2008. Sulfur isotope biogeochemistry of the Proterozoic McArthur Basin. Geochimica et Cosmochimica Acta 72 (17), 4278–4290.
Karlstrom, K.E., Åhäll, K.-I., Harlan, S.S., Williams, M.L., McLelland, J., Geissman, J.W., 2001. Long-lived (1.8–1.0 Ga) convergent orogen in southern Laurentia, its extensions to Australia and Baltica, and implications for refining Rodinia. Precambrian Research 111 (1–4), 5–30.
Kennedy, M., Droser, M., Mayer, L.M., Pevear, D., Mrofka, D., 2006. Late Precambrian oxygenation; inception of the clay mineral factory. Science 311 (5766), 1446–1449.
Kennedy, M.J., Pevear, D.R., Hill, R.J., 2002. Mineral surface control of organic carbon in black shale. Science 295 (5555), 657–660.
Killingley, J.S., 1983. Effects of diagenetic recrystallization on 18 O/16 O values of deep-sea sediments. Nature 301 (5901), 594–597.
Kirscher, U., Mitchell, R. N., Liu, Y., Nordsvan, A. R., Cox, G. M., Pisarevsky, S. A., Wang, C., Wu, L., Murphy, J. B., and Li, Z.-X., 2020, Paleomagnetic constraints on the duration of the Australia-Laurentia connection in the core of the Nuna supercontinent: Geology.
Knoll, A.H., Hayes, J.M., Kaufman, A.J., Swett, K., Lambert, I.B., 1986. Secular variation in carbon isotope ratios from Upper Proterozoic successions of Svalbard and East Greenland. Nature 321 (6073), 832–838.
Kositcin, N., and Carson, C., 2017, New SHRIMP U-Pb Zircon Ages from the Birrindudu and Victoria Basins, Northern Territory: July 2016-June 2017, Geoscience Australia.
Kovac, P., Titus, L., Cevallos, C., Bluett, J., 2014. Exploring for unconventional hydrocarbon plays in the Glyde Basin, Northern Territory, using FALCON® airborne gravity gradiometry (AGG) data. The APPEA Journal 54 (2), 519.
Krabbenhöft, A., Fietzke, J., Eisenhauer, A., Liebetrau, V., Böhm, F., Vollstaedt, H., 2009. Determination of radiogenic and stable strontium isotope ratios (87Sr/86Sr; δ88/86Sr) by thermal ionization mass spectrometry applying an 87Sr/84Sr double spike. Journal of Analytical Atomic Spectrometry 24 (9), 1267–1271.
Krabbenhöft, A., Eisenhauer, A., Böhm, F., Vollstaedt, H., Fietzke, J., Liebetrau, V., Augustin, N., Peucker-Ehrenbrink, B., Müller, M.N., Horn, C., Hansen, B.T., Nolte, N., Wallmann, K., 2010. Constraining the marine strontium budget with natural strontium isotope fractionations (87Sr/86Sr*, δ88/86Sr) of carbonates, hydrothermal solutions and river waters. Geochimica et Cosmochimica Acta 74 (14), 4097–4109.
Krassay, A., Bradshaw, B., Domagala, J., Jackson, M., 2000. Siliciclastic shoreline to growth-faulted, turbiditic sub-basins: the Proterozoic River Supersequence of the upper McNamara Group on the Lawn Hill Platform, northern Australia. Australian Journal of Earth Sciences 47 (3), 533–562.
Kump, L.R., Arthur, M.A., 1999. Interpreting carbon-isotope excursions: carbonates and organic matter. Chemical Geology 161 (1), 181–198.
Kunzmann, M., Schmid, S., Blaikie, T.N., Halverson, G.P., 2019. Facies analysis, sequence stratigraphy, and carbon isotope chemostratigraphy of a classic Zn-Pb host succession: The Proterozoic middle McArthur Group. McArthur Basin, Australia: Ore Geology Reviews 106, 150–175.
Kunzmann, M., Crombez, V., Catuneanu, O., Blaikie, T.N., Barth, G., Collins, A.S., 2020. Sequence stratigraphy of the ca. 1730 Ma Wollogorang Formation, McArthur Basin, Australia. Marine and Petroleum Geology 116, 104297.
Kunzmann, M., Crombez, V., Blaikie, T.N., Catuneanu, O., King, R., Halverson, G.P., Schmid, S., Spinks, S.C., 2022. Sequence stratigraphy of the ca 1640 Ma Barney Creek Formation, McArthur Basin, Australia. Australian Journal of Earth Sciences 1–29.
Kuznetsov, A.B., Melezhik, V.A., Gorokhov, I.M., Melnikov, N.N., Konstantinova, G.V., Kutyavin, E.P., Turchenko, T.L., 2010. Sr isotopic composition of Paleoproterozoic 13C-rich carbonate rocks: The Tulomozero Formation. SE Fennoscandian Shield: Precambrian Research 182 (4), 300–312.
Kuznetsov, A.B., Semikhatov, M.A., Gorokhov, I.M., 2018. Strontium Isotope Stratigraphy: Principles and State of the Art. Stratigraphy and Geological Correlation 26 (4), 367–386.
Land, L.S., 1995. Comment on "Oxygen and carbon isotopic composition of Ordovician brachiopods: Implications for coeval seawater" by H. Qing and J. Veizer. Geochimica et Cosmochimica Acta 59 (13), 2843–2844.
Large, R.R., Bull, S.W., Cooke, D.R., McGoldrick, P.J., 1998. A genetic model for the H.Y. C. Deposit, Australia; based on regional sedimentology, geochemistry, and sulfide-sediment relationships. Economic Geology 93 (8), 1345–1368.
Large, R.R., Bull, S.W., McGoldrick, P.J., 2000. Lithogeochemical halos and geochemical vectors to stratiform sediment hosted Zn–Pb–Ag deposits: Part 2. HYC deposit, McArthur River, Northern Territory: Journal of Geochemical Exploration 68 (1), 105–126.
R.R. Large S.W. Bull P.J. McGoldrick S. Walters G.M. Derrick G.R. Carr Stratiform and strata-bound Zn-Pb-Ag deposits in Proterozoic sedimentary basins 2005 northern Australia.
Large, D.E., Wolf, K.H., 1981. Sediment-hosted submarine exhalative lead-zinc deposits–a review of their geological characteristics and genesis: Handbook of strata-bound and stratiform ore deposits v. 9, 469–507.
Leach, D. L., Sangster, D. F., Kelley, K. D., Large, R. R., Garven, G., Allen, C. R., Gutzmer, J., and Walters, S., 2005, Sediment-hosted lead-zinc deposits: A global perspective.
Li, S.-S., Santosh, M., Farkaš, J., Redaa, A., Ganguly, S., Kim, S.W., Zhang, C., Gilbert, S., Zack, T., 2020. Coupled U-Pb and Rb-Sr laser ablation geochronology trace Archean to Proterozoic crustal evolution in the Dharwar Craton v. 343, 105709.
Liu, Y., Zhong, N., Tian, Y., Qi, W., Mu, G., 2011. The oldest oil accumulation in China: Meso-proterozoic Xiamaling Formation bituminous sandstone reservoirs. Petroleum Exploration and Development 38 (4), 503–512.
Lu, S., Zhao, G., Wang, H., Hao, G., 2008. Precambrian metamorphic basement and sedimentary cover of the North China Craton: A review. Precambrian Research 160 (1), 77–93.
Lyons, T.W., Gellatly, A.M., McGoldrick, P.J., Kah, L.C., 2006. Proterozoic sedimentary exhalative (SEDEX) deposits and links to evolving global ocean chemistry: Memoirs-Geological Society of. America 198, 169.
Lyons, T.W., Reinhard, C.T., Planavsky, N.J., 2014. The rise of oxygen in Earth's early ocean and atmosphere. Nature 506 (7488), 307–315.
P. McGoldrick P. Winefield S. Bull D. Selley R. Scott Sequences, synsedimentary structures, and sub-basins: the where and when of SEDEX zinc systems in the southern McArthur Basin 2010 Australia.
Medig, K.P.R., Thorkelson, D.J., Davis, W.J., Rainbird, R.H., Gibson, H.D., Turner, E.C., Marshall, D.D., 2014. Pinning northeastern Australia to northwestern Laurentia in the Mesoproterozoic. Precambrian Research 249, 88–99.
Millero, F.J., 1996. Chemical oceanography. CRC Press.
Mitchell, R.N., Kirscher, U., Kunzmann, M., Liu, Y., Cox, G.M., 2020. Gulf of Nuna: Astrochronologic correlation of a Mesoproterozoic oceanic euxinic event. Geology 49 (1), 25–29.
Morse, J., Luther III, G., 1999. Chemical influences on trace metal-sulfide interactions in anoxic sediments. Geochimica et Cosmochimica Acta 63 (19–20), 3373–3378.
Mozley, P.S., Wersin, P., 1992. Isotopic composition of siderite as an indicator of depositional environment. Geology 20, 817–820.
Munday, T., Sørensen, C., Marchant, D., Silic, J., Paterson, R., Viezzoli, A., Blaikie, T., and Spinks, S., An exploration of AEM inversion methods for defining sub-basin geometries in the McArthur Basin, Northern Territory, Australia.
Mukherjee, I., Large, R.R., 2020. Co-evolution of trace elements and life in Precambrian oceans: The pyrite edition. Geology 48 (10), 1018–1022.
Mukherjee, I., Large, R.R., Bull, S., Gregory, D.G., Stepanov, A.S., Ávila, J., Ireland, T.R., Corkrey, R., 2019. Pyrite trace-element and sulfur isotope geochemistry of paleo-mesoproterozoic McArthur Basin: Proxy for oxidative weathering. American Mineralogist 104 (9), 1256–1272.
Müller, P.J., Suess, E., 1979. Productivity, sedimentation rate, and sedimentary organic matter in the oceans—I. Organic carbon preservation. Deep Sea Research Part A. Oceanographic Research Papers 26 (12), 1347–1362.
Munson, T.J., Denyszyn, S.W., Simmons, J.M., Kunzmann, M., 2020. A 1642 Ma age for the Fraynes Formation, Birrindudu Basin, confirms correlation with the economically significant Barney Creek Formation, McArthur Basin, Northern Territory. Australian Journal of Earth Sciences 67 (3), 321–330.
Munson, T., 2019, Detrital zircon geochronology investigations of the Glyde and Favenc packages: Implications for the geological framework of the greater McArthur Basin, Northern Territory: in Annual Geoscience Exploration Seminar (AGES) Proceedings, Alice Springs, Northern Territory, 19–20 March 2019. Northern Territory Geological Survey, Darwin.
Nixon, A.L., Glorie, S., Collins, A.S., Blades, M.L., Simpson, A., Whelan, J.A., 2021. Inter-cratonic geochronological and geochemical correlations of the Derim Derim–Galiwinku/Yanliao reconstructed Large Igneous Province across the North Australian and North. Gondwana Research, China cratons.
Nordsvan, A.R., Collins, W.J., Li, Z.-X., Spencer, C.J., Pourteau, A., Withnall, I.W., Betts, P.G., Volante, S., 2018. Laurentian crust in northeast Australia: Implications for the assembly of the supercontinent Nuna. Geology 46 (3), 251–254.
Norris, A., Danyushevsky, L., 2018. Towards Estimating the Complete Uncertainty Budget of Quantified Results Measured by LA-ICP-MS: Goldschmidt: Boston. MA, USA.
NTGS., 2015, Final Well Completion Report, NT EP167, Manbulloo-S1: Australia, Northern Territory Geological Survey.

Oehler, J.H., 1977. Microflora of the HYC pyritic shale member of the Barney Creek Formation (McArthur Group), middle Proterozoic of northern Australia. Alcheringa 1 (3), 315–349.
Page, R.W., Sweet, I.P., 1998. Geochronology of basin phases in the western Mt Isa Inlier, and correlation with the McArthur Basin. Australian Journal of Earth Sciences 45 (2), 219–232.
Page, R.W., Jackson, M.J., Krassay, A.A., 2000. Constraining sequence stratigraphy in north Australian basins: SHRIMP U-Pb zircon geochronology between Mt Isa and McArthur River. Australian Journal of Earth Sciences 47 (3), 431–459.
Paytan, A., Griffith Elizabeth, M., Eisenhauer, A., Hain Mathis, P., Wallmann, K., Ridgwell, A., 2021. A 35-million-year record of seawater stable Sr isotopes reveals a fluctuating global carbon cycle. Science 371 (6536), 1346–1350.
Pietsch, B., 1991. Geological Map Series and Explanatory notes SE 53–03 1:, 2500000.
Piper, D.Z., Calvert, S.E., 2009. A marine biogeochemical perspective on black shale deposition. Earth-Science Reviews 95 (1), 63–96.
Piper, D., Perkins, R., 2004. A modern vs. Permian black shale—the hydrography, primary productivity, and water-column chemistry of deposition. Chemical geology 206 (3–4), 177–197.
Pisarevsky, S.A., Elming, S.-Å., Pesonen, L.J., Li, Z.-X., 2014. Mesoproterozoic paleogeography: Supercontinent and beyond. Precambrian Research 244, 207–225.
Plumb, K., Wellman, P., 1987. McArthur Basin, Northern Territory: mapping of deep troughs using gravity and magnetic anomalies. BMR Journal of Australian Geology & Geophysics 10 (3), 243–251.
Porter, T., 2017. McArthur River Zn-Pb-Ag deposit: Australasian Institute of Mining and Metallurgy. Monograph 32, 479–482.
Prokoph, A., Ernst, R.E., Buchan, K.L., 2004. Time-series analysis of large igneous provinces: 3500 Ma to present. The Journal of Geology 112 (1), 1–22.
Rafiei, M., Kennedy, M., 2019. Weathering in a world without terrestrial life recorded in the Mesoproterozoic Velkerri Formation: Nature. Communications 10 (1), 3448.
Rafiei, M., Löhr, S., Baldermann, A., Webster, R., Kong, C., 2020. Quantitative petrographic differentiation of detrital vs diagenetic clay minerals in marine sedimentary sequences: Implications for the rise of biotic soils. Precambrian Research 350, 105948.
Rawlings, D.J., 1999. Stratigraphic resolution of a multiphase intracratonic basin system: the McArthur Basin, northern Australia. Australian Journal of Earth Sciences 46 (5), 703–723.
Rawlings, D., 2002. Sedimentology, volcanology and geodynamics of the Redbank package, McArthur basin. University of Tasmania, northern Australia.
Redaa, A., Farkaš, J., Gilbert, S., Collins, A.S., Wade, B., Löhr, S., Zack, T., Garbe-Schönberg, D., 2021a. Assessment of elemental fractionation and matrix effects during in situ Rb–Sr dating of phlogopite by LA-ICP-MS/MS: implications for the accuracy and precision of mineral ages. Journal of Analytical Atomic Spectrometry.
Redaa, A., Farkaš, J., Hassan, A., Collins, A.S., Gilbert, S., Löhr, S.C., 2021b. Constraints from in-situ Rb-Sr dating on the timing of tectono-thermal events in the Umm Farwah shear zone and associated Cu-Au mineralisation in the Southern Arabian Shield, Saudi Arabia. Journal of Asian Earth Sciences, 105037.
Reinhard, C.T., Planavsky, N.J., Robbins, L.J., Partin, C.A., Gill, B.C., Lalonde, S.V., Bekker, A., Konhauser, K.O., Lyons, T.W., 2013. Proterozoic ocean redox and biogeochemical stasis. Proc Natl Acad Sci U S A 110 (14), 5357–5362.
Rousset, D., Leclerc, S., Clauer, N., Lancelot, J. l., Cathelineau, M., and Aranyossy, J.-F. o., 2004, Age and Origin of Albian Glauconites and Associated Clay Minerals Inferred from a Detailed Geochemical Analysis: Journal of Sedimentary Research, v. 74, no. 5, p. 631-642.
Sarmiento, J., Gruber, N., McElroy, M., Dynamics, O.B., 2007. Physics Today 60, 65.
Schidlowski, M., 1988. A 3,800-million-year isotopic record of life from carbon in sedimentary rocks. Nature 333 (6171), 313–318.
Schier, K., Himmler, T., Lepland, A., Kraemer, D., Schönenberger, J., Bau, M., 2021. Insights into the REY inventory of seep carbonates from the Northern Norwegian margin using geochemical screening. Chemical Geology 559, 119857.
Schmid, S., 2015, Sedimentological review of the Barney Creek Formation in drillholes LV09001, BJ2, McA5, McArthur Basin.
Schmitz, M.D., Schoene, B., 2007. Derivation of isotope ratios, errors, and error correlations for U-Pb geochronology using 205Pb-235U-(233U)-spiked isotope dilution thermal ionization mass spectrometric data. Geochemistry, Geophysics, Geosystems v. 8, no. 8.
C. Scott T.W. Lyons Contrasting molybdenum cycling and isotopic properties in euxinic versus non-euxinic sediments and sedimentary rocks: Refining the paleoproxies Chemical Geology v 2012 324–325, p. 19–27.
Scott, C., Lyons, T.W., Bekker, A., Shen, Y., Poulton, S.W., Chu, X., Anbar, A.D., 2008. Tracing the stepwise oxygenation of the Proterozoic ocean. Nature 452 (7186), 456–459.
Scott, C., Slack, J.F., Kelley, K.D., 2017. The hyper-enrichment of V and Zn in black shales of the Late Devonian-Early Mississippian Bakken Formation (USA). Chemical Geology 452, 24–33.
Selby, D., 2009. U-Pb zircon geochronology of the Aptian/Albian boundary implies that the GL-O international glauconite standard is anomalously young. Cretaceous Research 30 (5), 1263–1267.
Semikhatov, M., Kuznetsov, A., Gorokhov, I., Konstantinova, G., Melnikov, N., Podkovyrov, V., Kutyavin, E., 2002. Low 87Sr/86Sr ratios in seawater of the Grenville and post-Grenville time: determining factors. Stratigraphy and Geological Correlation 10 (1), 1–41.
Shalev, N., Gavrieli, I., Halicz, L., Sandler, A., Stein, M., Lazar, B., 2017. Enrichment of 88Sr in continental waters due to calcium carbonate precipitation. Earth and Planetary Science Letters 459, 381–393.
Shao, Y., Farkaš, J., Mosley, L., Tyler, J., Wong, H., Chamberlayne, B., Raven, M., Samanta, M., Holmden, C., Gillanders, B. M., Kolevica, A., and Eisenhauer, A., 2021, Impact of salinity and carbonate saturation on stable Sr isotopes (δ88/86Sr) in a lagoon-estuarine system: Geochimica et Cosmochimica Acta, v. 293, p. 461-476.
Sheldon, H.A., Schaubs, P.M., Blaikie, T.N., Kunzmann, M., Poulet, T., Spinks, S.C., 2021. 3D thermal convection in the Proterozoic McArthur River Zn-Pb-Ag mineral system, northern Australia. Ore Geology Reviews 133, 104093.
Shen, Y., Schidlowski, M., Chu, X., 2000. Biogeochemical approach to understanding phosphogenic events of the terminal Proterozoic to Cambrian: Palaeogeography. Palaeoclimatology, Palaeoecology 158 (1), 99–108.
Shen, Y., Canfield, D.E., Knoll, A.H., 2002. Middle Proterozoic ocean chemistry: Evidence from the McArthur Basin, northern Australia. American Journal of Science 302 (2), 81.
G. Shields J. Veizer Precambrian marine carbonate isotope database: Version 1.1 Geochemistry, Geophysics, Geosystems 3 6 2002 pp. 1 of 12–12 of 12.
Shields-Zhou, G., and Mills, B., 2017, Tectonic controls on the long-term carbon isotope mass balance: Proceedings of the National Academy of Sciences of the United States of America, v. 114.
Smith, J.B., 2001. Summary of results: joint NTGS-AGSO age determination program 1999–2001. Northern Territory Geological Survey Record 2001–007. https://geoscience.nt.gov.au/gemis/ntgsjspui/handle/1/82409.
Smith, B.R., 2016. Stratigraphic analysis of the Mainoru Formation. Northern Territory Geological Survey, Roper Group, McArthur Basin using HyLogger.
Southgate, P.N., Bradshaw, B.E., Domagala, J., Jackson, M.J., Idnurm, M., Krassay, A.A., Page, R.W., Sami, T.T., Scott, D.L., Lindsay, J.F., McConachie, B.A., Tarlowski, C., 2000. Chronostratigraphic basin framework for Palaeoproterozoic rocks (1730–1575 Ma) in northern Australia and implications for base-metal mineralisation. Australian Journal of Earth Sciences 47 (3), 461–483.
Spinks, S.C., Schmid, S., Pagès, A., 2016a. Delayed euxinia in Paleoproterozoic intracontinental seas: Vital havens for the evolution of eukaryotes? Precambrian Research 287, 108–114.
Spinks, S.C., Schmid, S., Pagés, A., Bluett, J., 2016b. Evidence for SEDEX-style mineralization in the 1.7 Ga Tawallah Group. McArthur Basin, Australia: Ore Geology Reviews 76, 122–139.
Spinks, S.C., Pearce, M.A., Liu, W., Kunzmann, M., Ryan, C.G., Moorhead, G.F., Kirkham, R., Blaikie, T., Sheldon, H.A., Schaubs, P.M., Rickard, W.D.A., 2021. Carbonate Replacement as the Principal Ore Formation Process in the Proterozoic McArthur River (HYC) Sediment-Hosted Zn-Pb Deposit, Australia. Economic Geology 116 (3), 693–718.
Spötl, C., Vennemann, T.W., 2003. Continuous-flow isotope ratio mass spectrometric analysis of carbonate minerals. Rapid Communications in Mass Spectrometry 17 (9), 1004–1006.
Stüeken, E.E., Gregory, D.D., Mukherjee, I., McGoldrick, P., 2021. Sedimentary exhalative venting of bioavailable nitrogen into the early ocean. Earth and Planetary Science Letters 565, 116963.
Subarkah, D., Blades, M. L., Collins, A. S., Farkaš, J., Gilbert, S., Löhr, S. C., Redaa, A., Cassidy, E., and Zack, T., 2021, Unraveling the histories of Proterozoic shales through in situ Rb-Sr dating and trace element laser ablation analysis: Geology.
Subarkah, D., Nixon, A.L., Jimenez, M., Collins, A.S., Blades, M.L., Farkaš, J., Gilbert, S. E., Holford, S., Jarrett, A., 2022. Constraining the geothermal parameters of in situ Rb–Sr dating on Proterozoic shales and their subsequent applications. Geochronology 4 (2), 577–600.
Sweet, I.P., Mendum, J.R., Bultitude, R.J., Morgan, C.M., 1974. The geology of the southern Victoria River region. Bureau of Mineral Resources, Geology and Geophysics, Northern Territor.
Tamblyn, R., Hand, M., Morrissey, L., Zack, T., Phillips, G., Och, D., 2020. Resubduction of lawsonite eclogite within a serpentinite-filled subduction channel. Contributions to Mineralogy and Petrology 175 (8), 74.
Tillberg, M., Drake, H., Zack, T., Kooijman, E., Whitehouse, M.J., Åström, M.E., 2020. In situ Rb-Sr dating of slickenfibres in deep crystalline basement faults: Scientific Reports 10, 562.
Tostevin, R., Shields, G.A., Tarbuck, G.M., He, T., Clarkson, M.O., Wood, R.A., 2016. Effective use of cerium anomalies as a redox proxy in carbonate-dominated marine settings. Chemical Geology 438, 146–162.
Tribovillard, N., Algeo, T.J., Lyons, T., Riboulleau, A., 2006. Trace metals as paleoredox and paleoproductivity proxies: An update. Chemical Geology 232 (1), 12–32.
Tyson, R., 2005. The“ productivity versus preservation” controversy: cause, flaws, and resolution: Special Publication-SEPM v. 82, 17.
Tyson, R.V., Pearson, T.H., 1991. Modern and ancient continental shelf anoxia: an overview: Geological Society. London, Special Publications 58 (1), 1–24.
Veizer, J., Plumb, K.A., Clayton, R.N., Hinton, R.W., Grotzinger, J.P., 1992. Geochemistry of Precambrian carbonates: V. Late Paleoproterozoic seawater: Geochimica et Cosmochimica Acta 56 (6), 2487–2501.
Veizer, J., Ala, D., Azmy, K., Bruckschen, P., Buhl, D., Bruhn, F., Carden, G.A., Diener, A., Ebneth, S., Godderis, Y., 1999. 87Sr/86Sr, δ13C and δ18O evolution of Phanerozoic seawater. Chemical geology 161 (1–3), 59–88.
Vermeesch, P., 2018. IsoplotR : A free and open toolbox for geochronology. Geoscience Frontiers v, 9.
Vinnichenko, G., Brocks, J.J., 2019. Results of a sampling study for LV09, MBXDD001, 14MCDDH001 and 14MCDDH002 drillcores. Australian National University, CSR0500.
Vinnichenko, G., Jarrett, A.J.M., Hope, J.M., Brocks, J.J., 2020. Discovery of the oldest known biomarkers provides evidence for phototrophic bacteria in the 1.73 Ga Wollogorang Formation 18, 544–559.
Vinnichenko, G., Jarrett, A.J., van Maldegem, L.M., Brocks, J.J., 2021. Substantial maturity influence on carbon and hydrogen isotopic composition of n-alkanes in sedimentary rocks. Organic Geochemistry 152, 104171.

Virgo, G.M., Collins, A.S., Amos, K.J., Farkaš, J., Blades, M.L., Subarkah, D., 2021. Descending into the "snowball": High resolution sedimentological and geochemical analysis across the Tonian to Cryogenian boundary in South Australia. Precambrian Research 367, 106449.

Vollstaedt, H., Eisenhauer, A., Wallmann, K., Böhm, F., Fietzke, J., Liebetrau, V., Krabbenhöft, A., Farkaš, J., Tomašových, A., Raddatz, J., Veizer, J., 2014. The Phanerozoic δ88/86Sr record of seawater: New constraints on past changes in oceanic carbonate fluxes. Geochimica et Cosmochimica Acta 128, 249–265.

Vorlicek, T.P., Helz, G.R., 2002. Catalysis by mineral surfaces: implications for Mo geochemistry in anoxic environments. Geochimica et Cosmochimica Acta 66 (21), 3679–3692.

Walker, R., Muir, M., Diver, W., Williams, N., Wilkins, N., 1977. Evidence of major sulphate evaporite deposits in the Proterozoic McArthur Group. Northern Territory, Australia: Nature 265 (5594), 526–529.

Walters, C.C., 2006. The Origin of Petroleum. Practical Advances in Petroleum Processing 79–101.

Wang, C., Deng, J., Carranza, E.J.M., Lai, X., 2014. Nature, diversity and temporal–spatial distributions of sediment-hosted Pb–Zn deposits in China. Ore Geology Reviews 56, 327–351.

Wang, C., Li, Z.-X., Peng, P., Pisarevsky, S., Liu, Y., Kirscher, U., Nordsvan, A., 2019. Long-lived connection between the North China and North Australian cratons in supercontinent Nuna: paleomagnetic and geological constraints. Science Bulletin 64 (13), 873–876.

Wanty, R.B., Goldhaber, M.B., 1992. Thermodynamics and kinetics of reactions involving vanadium in natural systems: Accumulation of vanadium in sedimentary rocks. Geochimica et Cosmochimica Acta 56 (4), 1471–1483.

Wenzhi, Z., Suyun, H., Zecheng, W., Zhang, S., Tongshan, W., 2018. Petroleum geological conditions and exploration importance of Proterozoic to Cambrian in China. Petroleum Exploration and Development 45 (1), 1–14.

Wilson, S.A., 1997. United States Geological Survey Certificate of Analysis Basalt. U.S Geological Survey, Columbia River BCR-2.

P. Winefield Sedimentology and diagenesis of late palaeoproterozoic carbonates, Southern McArthur Basin 1999 northern Australia.

P.R. Winefield Development of late Paleoproterozoic aragonitic seafloor cements in the McArthur Group 2000 northern Australia.

Woodhead, J. D., and Hergt, J. M., 2001, Strontium, Neodymium and Lead Isotope Analyses of NIST Glass Certified Reference Materials: SRM 610, 612, 614: Geostandards Newsletter, v. 25, no. 2-3, p. 261-266.

Wright, J., 1995. Seawater: its composition, properties, and behaviour. Pergamon.

Xu, G., Hannah, J.L., Bingen, B., Georgiev, S., Stein, H.J., 2012. Digestion methods for trace element measurements in shales: Paleoredox proxies examined. Chemical Geology v. 324–325, 132–147.

B. Yang A. Collins M. Blades N. Capogreco J. Payne T. Munson G. Cox S. Glorie Middle-late Mesoproterozoic tectonic geography of the North Australia Craton: U-Pb and Hf isotopes of detrital zircon grains in the Beetaloo Sub-basin, Northern Territory, Australia Journal of the Geological Society 176 2019 p. jgs2018-2159.

B. Yang A.S. Collins G.M. Cox A.J.M. Jarrett S. Denyszyn M.L. Blades J. Farkaš S. Glorie . v. n, a, no. n, a. Using Mesoproterozoic Sedimentary Geochemistry to Reconstruct Basin Tectonic Geography and Link Organic Carbon Productivity to Nutrient Flux from a Northern Australian Large Igneous Province: Basin Research 2020.

Yang, B., Smith, T.M., Collins, A.S., Munson, T.J., Schoemaker, B., Nicholls, D., Cox, G., Farkas, J., Glorie, S., 2018. Spatial and temporal variation in detrital zircon age provenance of the hydrocarbon-bearing upper Roper Group. Beetaloo Sub-basin, Northern Territory, Australia: Precambrian Research 304, 140–155.

Yang, B., Collins, A.S., Blades, M.L., Munson, T.J., Payne, J.L., Glorie, S., Farkaš, J., 2022. Tectonic controls on sedimentary provenance and basin geography of the Mesoproterozoic Wilton package. McArthur Basin, northern Australia: Geological Magazine 159 (2), 179–198.

Yano, M., Yasukawa, K., Nakamura, K., Ikehara, M., Kato, Y., 2020. Geochemical Features of Redox-Sensitive Trace Metals in Sediments under Oxygen-Depleted Marine Environments, Minerals Volume 10.

Zhang, S.-H., Ernst, R.E., Pei, J.-L., Zhao, Y., Zhou, M.-F., Hu, G.-H., 2018. A temporal and causal link between ca. 1380 Ma large igneous provinces and black shales: Implications for the Mesoproterozoic time scale and paleoenvironment. Geology 46 (11), 963–966.

Zhang, S.-H., Zhao, Y., Li, X.-H., Ernst, R. E., and Yang, Z.-Y., 2017, The 1.33–1.30 Ga Yanliao large igneous province in the North China Craton: Implications for reconstruction of the Nuna (Columbia) supercontinent, and specifically with the North Australian Craton: Earth and Planetary Science Letters, v. 465, p. 112-125.

Zhang, S.-H., Ernst, R. E., Munson, T. J., Pei, J., Hu, G., Liu, J.-M., Zhang, Q.-Q., Cai, Y.-H., and Zhao, Y., 2021, Comparisons of the Paleo-Mesoproterozoic large igneous provinces and black shales in the North China and North Australian cratons: Fundamental Research.

Zhang, W., Xu, W., Liu, P., Liu, C., and Liu, F., 2022, Eastern North China Craton–North Australia Craton connection at 1.0 Ga through detrital zircon mixing modelling: Terra Nova, v. n/a, no. n/a.

Zhang, S., Li, Z.-X., Evans, D.A.D., Wu, H., Li, H., Dong, J., 2012. Pre-Rodinia supercontinent Nuna shaping up: A global synthesis with new paleomagnetic results from v. 353–354, 145–155.

Zhang, K., Shields, G.A., 2022. Sedimentary Ce anomalies: Secular change and implications for paleoenvironmental evolution. Earth-Science Reviews 229, 104015.

Zhao, G., Sun, M., Wilde, S.A., Li, S., 2004. A Paleo-Mesoproterozoic supercontinent: assembly, growth and breakup. Earth-Science Reviews 67 (1–2), 91–123.